

UNIVERSITY OF ARIZONA

AEROSPACE AND MECHANICAL ENGINEERING

AME 401

Subsonic Experiments Final Report

Group G

By Theo Altneu, Tyler Cook, Reed Spurling, Gavin Vetro, Carly Wingness

10/19/2024

SUMMARY

This document is the collection of information gathered from a series of subsonic wind tunnel experiments conducted in the University of Arizona (UA) AeroLab tunnel under the guidance of Dr. James Threadgill and the supervision of his Teaching Assistant, Adrien Bouskela. The experiments include an analysis of the uniformity and turbulence of the wind tunnel so that a calibration can be made to confirm the reliability of future experiments as well as the aerodynamic forces on a cylinder and Clark Y-14 airfoil using pressure along the surface and the wake, and the measurement of aerodynamic forces on a wing section using a sting balance with the addition of a slat and a flap. It was found that as the experiments increased their complexity in terms of configuration and data collection, more information was able to be determined from the flow over the model. The over goal of the experiment was to analyze different models and measurement techniques to develop skills in subsonic wind tunnel testing.

NOMENCLATURE

<u>Symbol</u>	<u>Name</u>	<u>Units</u>
c	Chord	(m)
C_A	Coefficient of Axial Force	-
C_D	Coefficient of Drag	-
C_L	Coefficient of Lift	-
$C_{M,LE}$	Coefficient of Moment about leading edge	-
$C_{M,c/4}$	Coefficient of Moment about quarter chord	-
C_N	Coefficient of Normal Force	-
C_P	Coefficient of Pressure	-
C_{Pl}	Coefficient of Pressure on the lower wing surface	-
C_{Pu}	Coefficient of Pressure on the upper wing surface	-
D	Drag	(N)
L	Lift	(N)
M	Moment	(N·m)
P	Pressure	(mbar) (Pa)
P_0	Stagnation Pressure	(mbar) (Pa)
P_∞	Freestream Pressure	(mbar) (Pa)

q	Dynamic Pressure	(mbar) (Pa)
R	Radius	(in) (m)
Re	Reynolds Number	-
S	Reference Area	(m ²)
u'	RMS of Velocity Fluctuations	(m/s)
\overline{u}	Time-Averaged Velocity	(m/s)
V	Air Velocity	(m/s)
V_{∞}	Freestream Air Velocity	(m/s)
y	Rake Distance	(m)
α	Angle of Attack	(°)
ρ	Air Density	(kg/m ³)
ν	Dynamic Viscosity	(Pa·s)

INTRODUCTION

This report describes a series of subsonic wind tunnel experiments conducted in the University of Arizona (UA) AeroLab tunnel under the guidance of Dr. James Threadgill and the supervision of his Teaching Assistant, Adrien Bouskela. The experiments performed in the lab aim to inform undergraduate aerospace engineering students how to utilize and perform tasks in a subsonic wind tunnel.

In the first experiment, it is sought to understand the performance of the wind tunnel as a function of fan speed. Wind tunnels experience turbulence and nonuniformities that may affect the performance of the tunnel, so a method of calibration to confirm the accuracy of the set-up of future experiments needs to be created. Following experiments focus on recording pressure measurements around a cylinder and a wing section to discover aerodynamic force characteristics. This allows an understanding of how pressure-based measurements are made and used in practical applications. Pressure is recorded on the cylinder and the wing section using pressure taps for experiments 2 and 3. Experiment 4 expanded on the previous two by using a set of pitot static probes in the wake of the wing section. This allows a comparison on different types of drag and creates various solution methods to solve for drag on a wing. Finally, a force balance is used to directly measure the aerodynamic forces and pitching moment on an airfoil. Becoming familiar with this technique allows for a direct comparison of the results obtained from a force balance to the results obtained from pressure distributions. The reliability of the experiments and data collected can then be confirmed.

This report contains a methods section that describes the setup and conditions of all experiments performed, a results section that contains the theoretical development and the processed data, and it concludes with a discussion and comparison of the results obtained. There are also references and appendices of the data collected attached.

The experiments described in this report have been performed before by previous classes and by other groups of students in the current semester's class. Therefore, the experimental methods and analyses described are not new, but are still useful for expanding skills and knowledge about subsonic wind tunnel testing.

EXPERIMENTAL METHODS

All experiments described in this document are tested in the University of Arizona (UA) AeroLab Educational Wind Tunnel. This is an Open-Circuit, subsonic wind tunnel containing a square profile test section of 12x12x24 inches. The tunnel is located in Tucson, Arizona, and testing is performed at an ambient room temperature of 23°C and a density of 1.085 kg/m³.

Experiment 1 utilized a pitot-static probe and a hot-wire anemometer. Dynamic pressure and voltage were recorded at a logarithmic increment of fan speed from 0% to 50%. These sensor readings were then compared to the AEROLAB integrated sensors, allowing for the calculation of a calibration curve and a turbulence intensity factor for several fan speed settings. The pitot-static tube, with a sensor accuracy of $\pm 0.08\%$ of reading [1], was mounted onto the wall of the test section. The hot-wire anemometer was mounted on the test section wall opposite of the pitot-static tube.

Experiment 2 verified the reliability of the tunnel by testing the calibration curve from Experiment 1 on a 4" (0.1016 m) diameter cylinder. Pressure taps spaced evenly every 15° along the circumference of the cylinder were used to create a pressure profile, which is later used to calculate the total drag of the cylinder, as well as the locations of separation, maximum velocity, and where the pressure matched the freestream pressure, at various Reynolds numbers for comparison with past accepted results. Additionally, a run was conducted with trip-strips applied to simulate Reynolds numbers beyond the capacity of the tunnel. The well documented flow behavior of a circular cylinder provided essential testing grounds for future experiments where the flow behavior may not be so easily predictable.

Experiments 3, 4, and 5 utilize a Clark Y-14 wing section with a chord length of 3.5" (0.0889 m) and a span of 9.875" (0.251 m).

In Experiment 3, used pressure taps were used to measure the pressure (C_p) distribution over the surface of a Clark Y-14 airfoil (Fig. 1) over a range of angles of attack ($\alpha = -4^\circ$ – 20°) at a Reynolds number of $Re = 100,000$. The data was analyzed to find the locations of flow stagnation and separation points, and to calculate lift (c_l), drag (c_d), and pitching moment (c_m) on the airfoil. Experiment 3, unlike Experiment 4, did not measure or account for skin friction drag.

Experiment 4 utilized and consequently expanded on the findings from the previous experiments. The fourth section of the experiment took the findings regarding the skin drag on the airfoil, and added another dimension in the form of pressure drag to help begin to form a more complete picture of the drag profile. By utilizing a set of 18 pitot static probes spaced ¼" apart from each other, the pressure distribution was able to be measured across the airfoil's wake. This pressure distribution was then measured for varying angles of attack from -4° to 14° , and helped give a more accurate picture of drag being measured on the Clark Y-14 airfoil.

Experiment 5 continues using the Clark Y-14 wing section with the addition of a 3/16" slat and a split flap deflected 45° . It is mounted on a sting balance that records normal force, axial force, and pitching moment about its center. The center of the balance is approximately 0.04097 m from the aerodynamic center of the Clark Y-14. Forces and pitching moments were recorded for angles of attack of -4° to 20° by increments of 2° . Data was recorded for four different cases: one without a slat or flap, one with the slat, one with the flap deflected, and one with the slat and flap.

RESULTS

A comparison between the AEROLAB data and the pitot-static tube data must be made to create a correction factor between the true pressure (from the pitot-static tube) and the AEROLAB pressure. This is done in terms of average pressure in Figure (1) and in terms of average velocity in Figure (2).

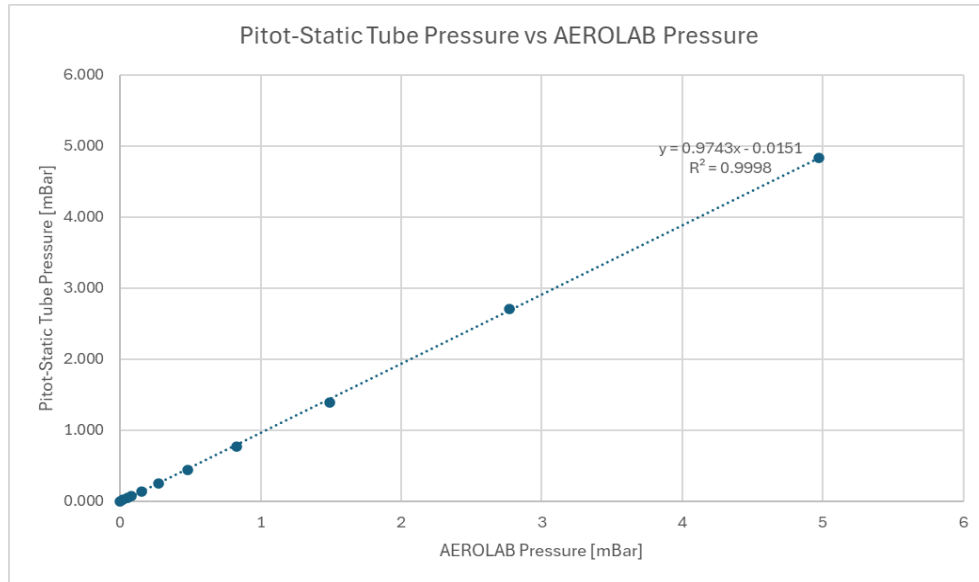


Figure (1) Results from the pitot-static tube as a function of AEROLAB's recorded pressure.

The velocity can be calculated using Bernoulli's equation from the recorded pitot-static tube dynamic pressure.

$$V = \sqrt{\frac{2(P_0 - P)}{\rho}} \quad (1)$$

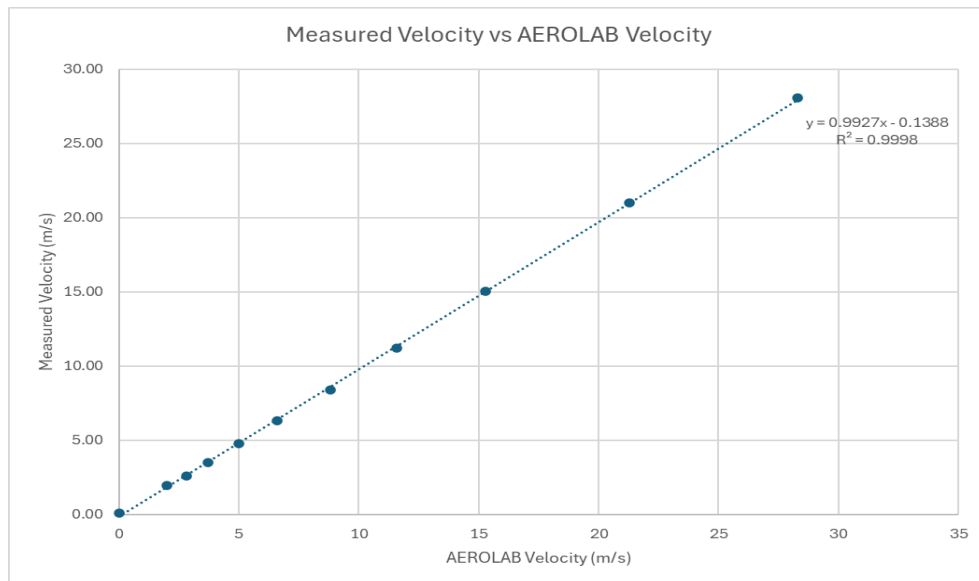


Figure (2) Velocity as a function of AEROLAB's recorded velocity.

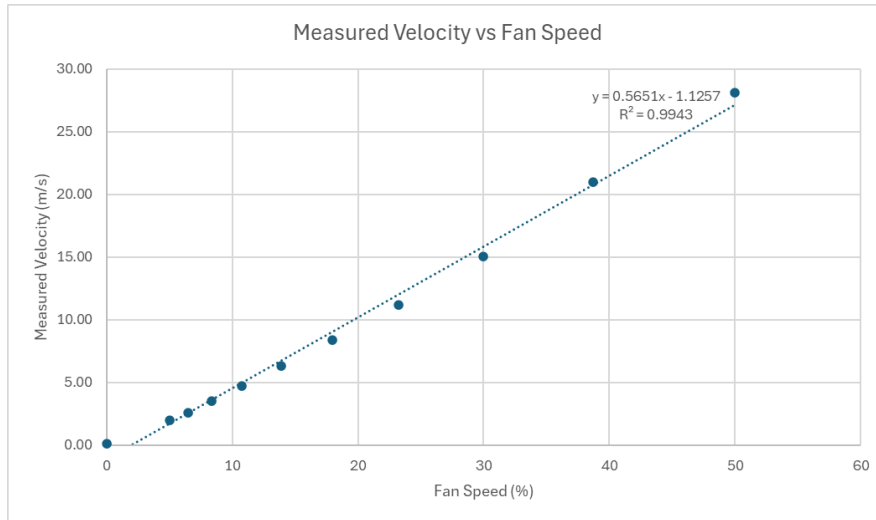


Figure (3) Velocity as a function of fan speed setting.

From the linear trendline fits in Figures (2) and (3), a calibration factor can be found that allows all future experiments to be based on the pitot-static tube pressure.

$$y = 0.9743x - 0.0151 \quad (2)$$

$$y = 0.9927x - 0.1388 \quad (3)$$

Equation 2 is from the pressure plot, and Equation 3 is from the velocity plot. The desired pressure or velocity is plugged in for 'y' value, and the pressure or velocity that AEROLAB displays is given by the 'x' value.

The hot-wire anemometer's data output is in terms of Volts. First, a calibration curve must be obtained, fitting a 4th order polynomial to the plot of freestream velocity from the pitot-static tube as a function of volts [2].

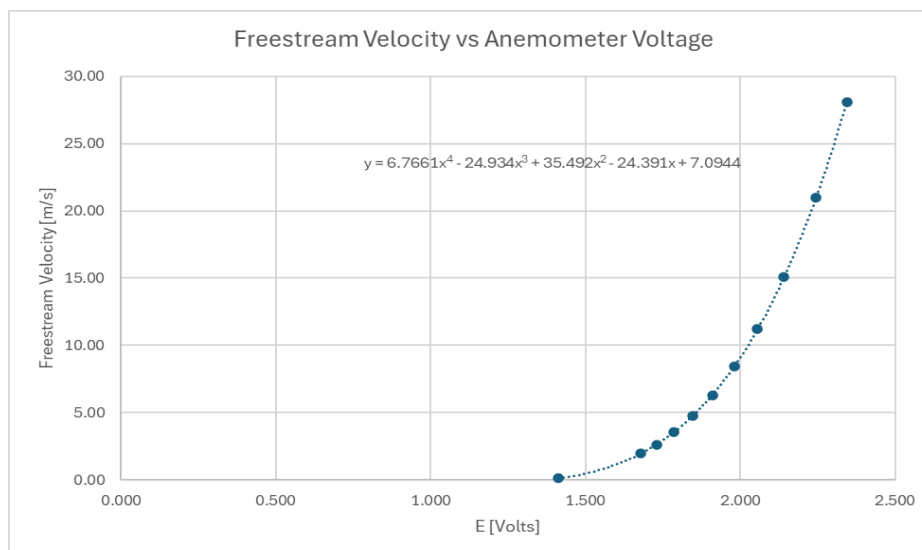


Figure (4) Anemometer calibration curve, velocity as a function of voltage.

From the anemometer's voltage data, the turbulence intensity can then be calculated using this equation.

$$T.I. = \sqrt{\frac{(u')^2}{u}} \quad (4)$$

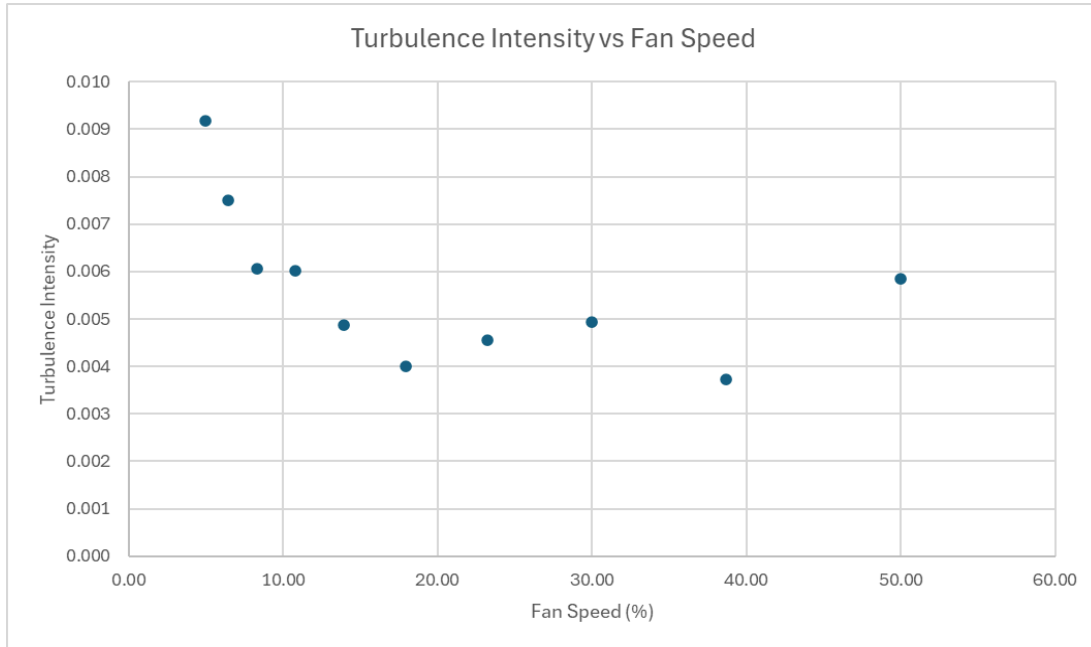


Figure (5) Turbulence Intensity at several fan speed settings.

The turbulence intensity is calculated using 200,000 data points at all selected fan speed settings.

To begin the experiments involving the cylinder and the Clark Y-14, the tunnel needs to be calibrated according to the results found in Experiment 1.

With the dynamic pressure calibration curve obtained, Experiment 2 could now begin, studying the flow around a circular cylinder. Data recorded at pressure taps on the surface of the cylinder was saved as a series of pressure coefficients for each point. The first action in interpreting these results was to convert the pressure coefficients into values of surface pressure.

$$P = C_p q_\infty + P_\infty \quad (5)$$

From this, the maximum value of velocity can be found by rearranging Bernoulli's formula.

$$V = \sqrt{\frac{2(P_0 - P)}{\rho}} \quad (6)$$

Pressure and velocity were calculated for each point individually, but calculating drag takes every value of pressure around the cylinder into account. Drag is ideally given by:

$$D = - \int_0^{2\pi} P \cdot R \cos(\theta) d\theta \quad (7)$$

However, due to the discrete nature of the data recorded, a more pragmatic method was used to calculate drag involving the trapezoidal method of interpolation.

$$\sum D = \sum_0^n \frac{D_n + D_{n+1}}{2R} \frac{\pi}{24} \quad (8)$$

$$D_n = P_n \cos(\theta_n) \quad (9)$$

Drag was then converted to a coefficient of drag using the definition of C_D .

$$C_D = \frac{D}{q_\infty S} \quad (10)$$

	q (mbar)	Separation (°)	P = P _∞ (°)	Max V (m/s)	C _D
Untripped Re = 50k	0.369	±55°	46°	12.30	1.07
Untripped Re = 100k	1.48	±60 - 65°	45°	25.16	1.27
Untripped Re = 150k	3.32	±65 - 70°	45°	37.50	1.11
Tripped Re = 150k	3.32	±75 - 80°	43°	41.17	0.54

Table (1) Results from calculation displaying where the flow separated, pressure matched the freestream pressure, value of max velocity, and drag coefficient for the Reynolds numbers tested.

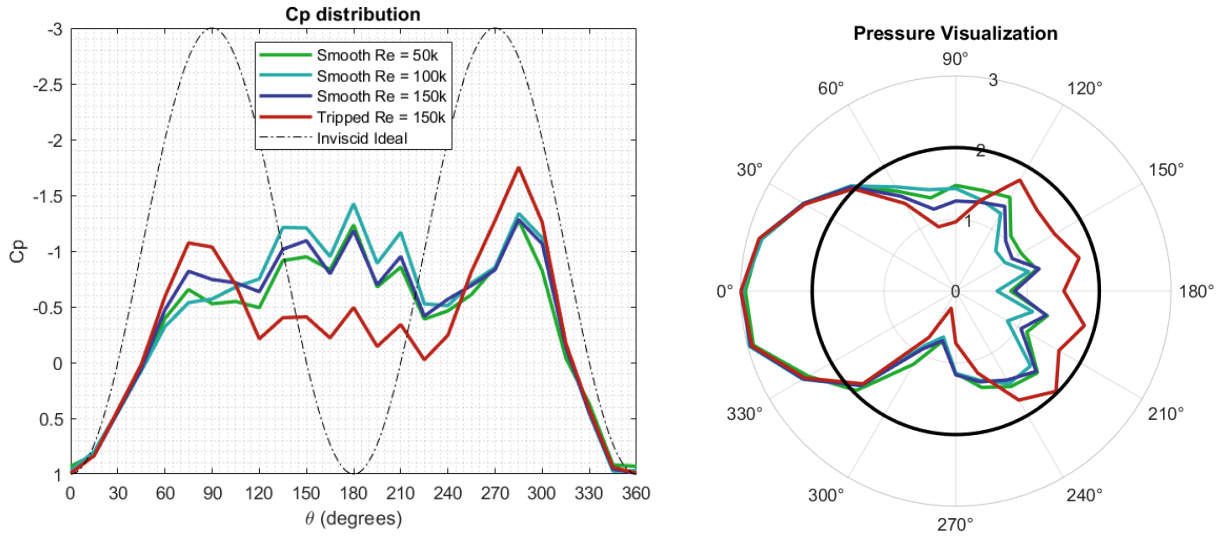


Figure (6) Pressure Distribution around the cylinder for various Reynolds Numbers. NOTE in the data at $\theta=30^\circ$ the recorded C_p was greater than 1, which implies that that tap was malfunctioning. To correct for this in calculation, that point was removed.

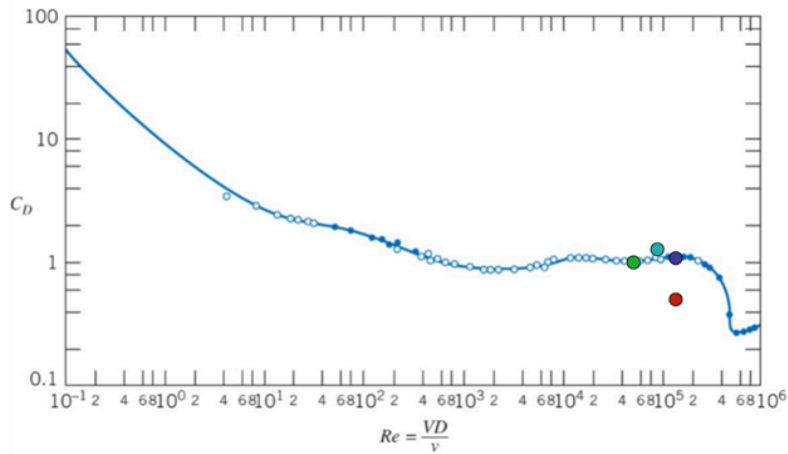


Figure (7) Drag Coefficient with respect to Reynolds Number for a circular cylinder. The colored dots correspond to the C_D values calculated during this experiment.

Locations for the max velocity, pressure, and separation are all estimates made by interpolating the data. Since there is a 15° gap between points on the cylinder, precise locations of these values are unknown. A larger uncertainty is granted to the location of flow separation because there is no applicable equation to determine where flow will separate.

From the pressure distribution in Figure (6), the effects of viscosity can be seen. Note the dashed line represents the inviscid pressure distribution from incompressible potential flow theory. To model a cylinder in inviscid flow, a doublet (source and sink) placed in uniform flow is all that is needed, and leads to the following equation for C_p .

$$C_p = 1 - 4\sin^2(\theta) \quad (11)$$

Between roughly 60° and 300° , the pressure data diverges from the inviscid theory as viscous effects kick in and the flow separates from the surface, leaving a recirculating bubble clinging to the rear of the cylinder. This bubble is the most prominent source of drag, however, the contributions from skin friction and 3D effects are missing, which cannot be captured by this data; these topics will be discussed in later experiments.

The inviscid theory is more closely captured by the tripped $Re = 150k$ case, where the flow is forced into turbulence at about $\pm 30^\circ$, releasing potential energy as kinetic and allowing the flow to stay attached longer. This decreases the size of the separation bubble, thus decreasing drag significantly (see Table (1)). By forcing the transition of the airflow from laminar to turbulent, a much higher Reynolds number is essentially simulated, which explains the outlying C_D point in Figure (7).

There is one meticulous detail to notice from Figure (6), and that is that between all the Reynolds numbers, the pressure on the bottom half of the cylinder consistently followed the inviscid case more closely than the top half. Since this is not only true for these results, but for the results of other groups conducting the same experiment in this tunnel as well, it can be inferred that some inherent asymmetry is present. This could come from the cylinder being possibly misaligned, a pressure leak near the model, the behavior of airflow entering the inlet (due to imperfections in the inlet honeycomb or its proximity to a wall on one side), the vortex generated by the driving fan propagating upstream, or something else. Where this asymmetry comes from cannot be determined without further investigation, but it is worthy of note for future reference.

Experiment 3 built on Experiment 2, using the same pressure measurement system on a Clark Y-14 airfoil instead of a cylinder. C_p is plotted across the airfoil surface at each angle of attack (Fig. 8), and inspected these plots to identify the flow stagnation points (where $C_p \approx 1$, and the pressure matches that in a Pitot tube pointed directly into the flow), and flow separation points along the top surface of the airfoil. This shows that flow stagnation points occurred at or near the leading edge of the airfoil, moving a small distance down onto the front of the bottom surface of the airfoil at high angles of attack. This shows that flow separation occurred near the back of the upper surface of the airfoil at lower positive angles of attack, moving towards the leading edge at higher angles of attack.

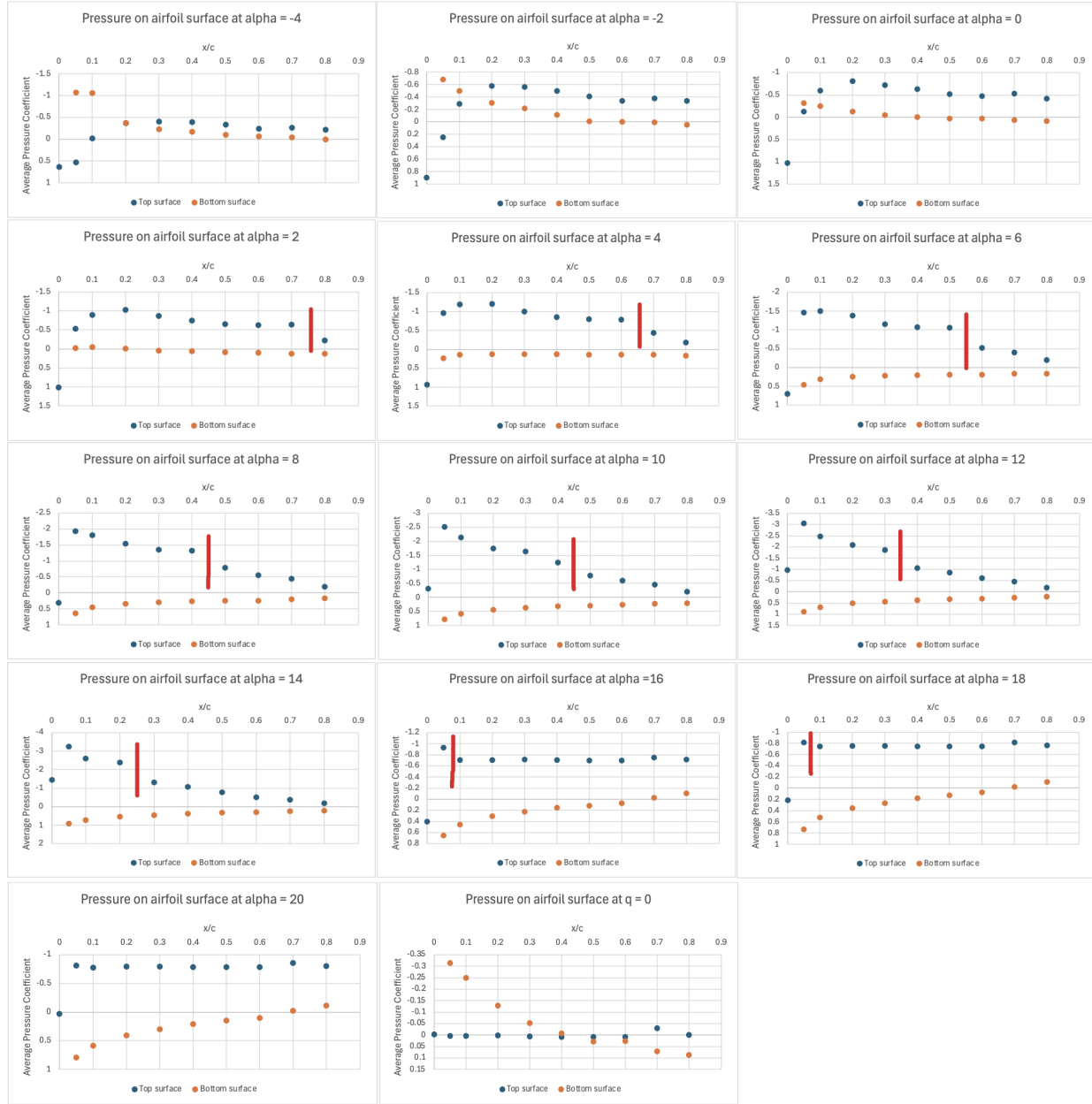


Figure (8) Pressure coefficients across the airfoil surface from $\alpha = -4^\circ$ – 20° , as well as a set of pressure coefficients measured when the tunnel was not running ($q = 0$), for comparison. Apparent flow separation locations are marked by red lines. Data from Experiment 3. Standard deviations provided in data sheet appendix.

After measuring these C_p distributions, they are used to calculate lift (C_l), drag (C_d), and pitching moment (C_m). As an intermediate step, the normal and axial force coefficients on the airfoil are calculated at each α using trapezoidal approximations of equations 12 and 13, respectively,

$$C_A = \frac{1}{c} \int_{x=0}^{x=c} (C_{P,u} - C_{P,l}) dy \quad (12)$$

$$C_N = \frac{-1}{c} \int_{x=0}^{x=c} (C_{P,u} - C_{P,l}) dx \quad (13)$$

where $C_{P,u}$ is the pressure coefficient at x/c along the airfoil's upper surface, and $C_{P,l}$ is the pressure coefficient at x/c along the airfoil's lower surface.

Lift and drag are relative to the airflow, not the airfoil, so coordinate transformations are performed to find C_l and C_d using equations 14 and 15, respectively.

$$C_L = C_N \cos(\alpha) - C_A \sin(\alpha) \quad (14)$$

$$C_D = C_N \sin(\alpha) + C_A \cos(\alpha) \quad (15)$$

The moment about the airfoil's leading edge, $C_{M,LE}$, is calculated by using a trapezoidal approximation of Eq 16. Note that this formulation of Eq. 16 does not account for frictional forces.

$$C_{M,LE} = \frac{1}{c^2} \left[\int_{x=0}^{x=c} (C_{P,u} - C_{P,l}) x dx + \int_{x=0}^{x=c} C_{P,u} \frac{dy_u}{dx} y_u dx - \int_{x=0}^{x=c} C_{P,l} \frac{dy_l}{dx} y_l dx \right] \quad (16)$$

Then the calculated lift, drag, and moment coefficients are plotted as a function of α , in addition to the drag polar in Fig. 9, below.

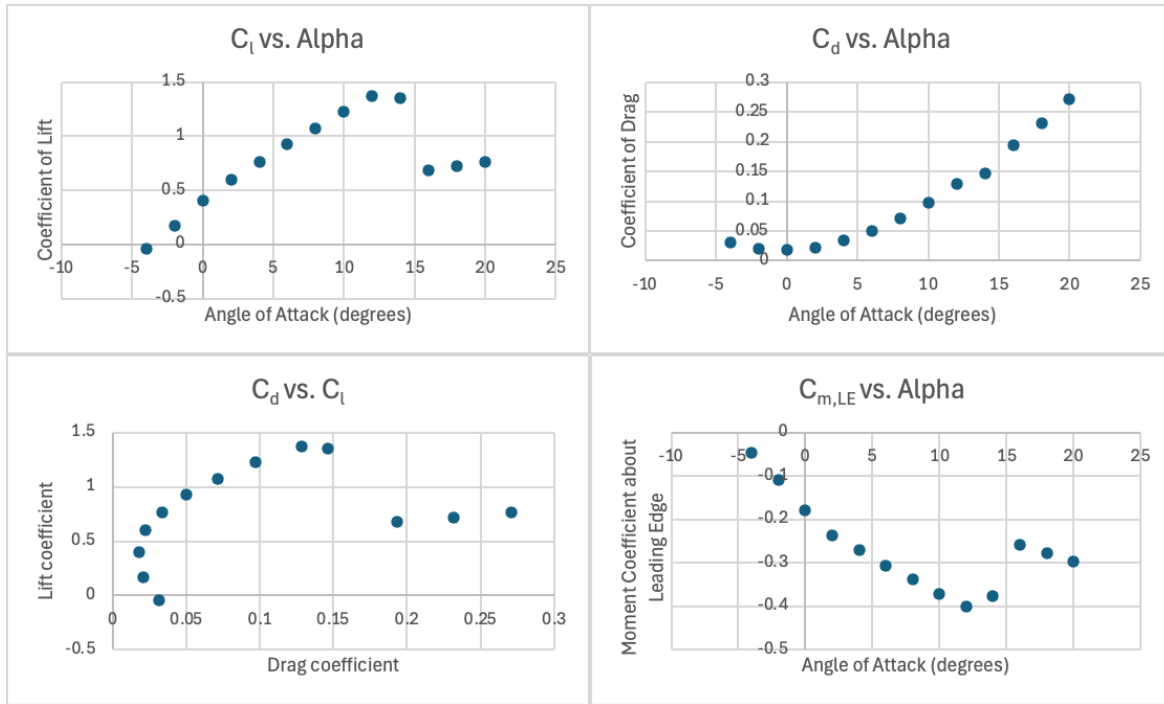


Figure (9) C_L vs. α , C_d vs. α , C_d vs C_L (drag polar), and $C_{M,LE}$ vs. α from A3.

The entirety of the fourth experiment was done with the explicit goal of determining the coefficient of drag in the wake of the airfoil, so the natural first step was to determine the equation with which all future determinations would be made:

$$C_d = 2 \int \sqrt{\frac{q_{data}}{q_{\infty,New}}} - \frac{q_{data}}{q_{\infty,New}} d\left(\frac{y}{c}\right) \quad (17)$$

This equation is derived via closed system analysis of the test section of the wind tunnel, which comes from the principles of conservation of mass and momentum. The following image represents the control volume through which the analysis is conducted, with the airfoil simplified as a cylinder:

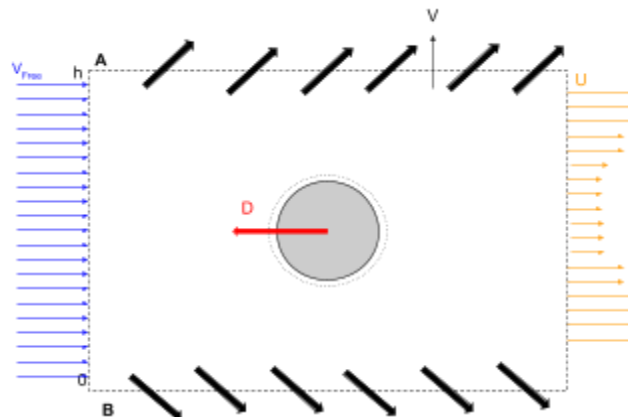


Figure (10) Closed Volume System

The integral around the entire surface in the control volume must be equal to that out of the control volume, totaling to 0, therefore obtaining the following two equations, the first of which is conservation of mass, and the second of which is the conservation of momentum.

$$0 = \int_{CV} \rho dV + \int_{CS} \rho \bar{v} \cdot d\bar{A} \quad (18)$$

$$\bar{F} = \int_{CV} \bar{v} \rho dV + \int_{CS} \bar{v} \rho \bar{v} \cdot d\bar{A} \quad (19)$$

The control volume (CV) portions of both of these integrals become 0. By referencing the diagram it can be seen that the two control surface (CS) portions respectively become:

$$0 = \int_0^h \rho v_{\infty} dy + \int_0^h \rho u dy + \int_A \rho v dA + \int_B \rho v dB \quad (20)$$

$$-D = \int_0^h -v_{\infty} \rho v_{\infty} dy + \int_0^h u \rho u dy + \int_{AB} u_{\infty} \rho v dAB \quad (21)$$

By combining like terms and putting the integrals together the following equation is achieved:

$$-D = \int_0^h -\rho v_{\infty}^2 + \rho u^2 + \rho v_{\infty}^2 - \rho u v_{\infty} dy \quad (22)$$

Which can be further simplified as follows:

$$-D = \int_0^h \rho u(u - v_{\infty}) dy \quad (23)$$

The next step is to replace ‘u’ the dynamic pressure, q, and v_{∞} as the free stream dynamic pressure, q_{∞} . Upon nondimensionalization of this equation, Equation 17 is obtained.

During this portion of the experiment, C_p in the wake of the airfoil was measured, so the goal was to take these measured values and turn them into quantities that could be utilized in the aforementioned equation 23. This occurs beginning by looking at the definition of the coefficient of pressure, which stems from a rearranged version of equation 5:

$$C_p = \frac{p - p_{\infty}}{q_{\infty}} \quad (24)$$

The dynamic pressure is multiplied over and defined as the new freestream dynamic pressure ($q_{\infty, New}$):

$$C_{p, Stagnation} q_{\infty} = p - p_{\infty} = q_{\infty, New} \quad (25)$$

C_p is then divided by the stagnation C_p , (this ratio is referred to as $C_{p,Normal}$) which can be assumed to occur at the first pitot-static tube rake position, which normalizes the data such that the first point always has a C_p reading of 1. This results in the following equation:

$$C_{p,Normal} = \frac{p_{data}}{q_{\infty} C_{p,stagnation}} \quad (26.1/26.2)$$

$$\Rightarrow C_{p,Normal} = \frac{p_{data}}{q_{\infty,New}}$$

If p_{data} is considered to be the dynamic pressure in the system, then:

$$C_{p,Normal} = \frac{q_{data}}{q_{\infty,New}} \quad (27)$$

This ultimately means that this $C_{p,Normal}$ ratio can be plugged directly into equation 16 as this was the final goal in the data analysis. The only thing left to do in the data analysis is take the infinite integral that was found from control volume analysis, and turn it into a summation that can be used with discrete data points. This results in the following:

$$C_d = 2 \sum \sqrt{C_{p,Normal}} - C_{p,Normal} \frac{\Delta y}{c} \quad (28)$$

With all of these considerations made, the coefficient of drag can be produced for each angle of attack, which results in the following graph.

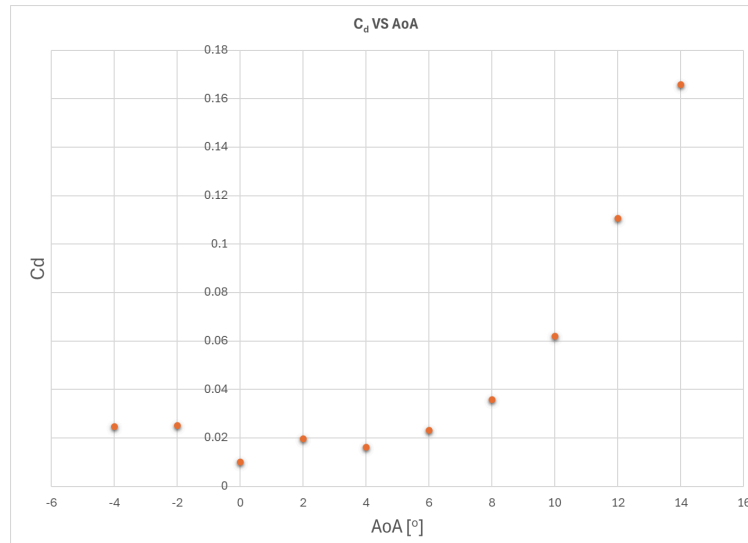


Figure (11) shows the relationship between the coefficient of drag and the angle of attack.

Another massive component of this portion of the experiment was to compare the results acquired here with the results from the previous section, and this overlay results in the following graph:

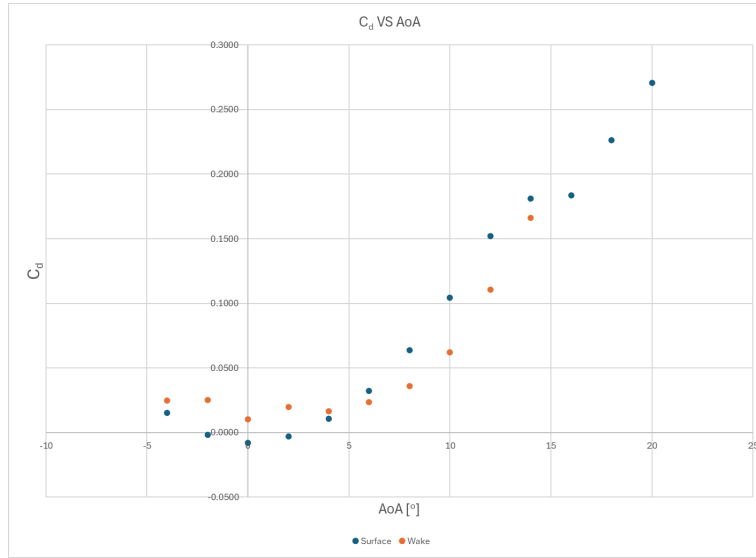


Figure (12) Section A3 (Blue) & A4 (Orange) C_d vs α .

This figure demonstrates the similarities in trends between the two experimental methods. This concludes the results for the wake inspection portion of the experiment.

Experiment 5 utilized the same methods as A3 and A4 to find the dynamic pressure calibration from A1 for a wing section, which resulted in a dynamic pressure of 1.98 mbar to set the fan power. To use the forces and moments from the sting balance, they need to be adjusted for the angle of attack and moment position. These forces are derived by:

$$L = N \cos \alpha - A \sin \alpha \quad (29)$$

where L is the lift force, N is the normal force, A is the axial force, and α is the angle of attack.

$$D = N \sin \alpha + A \cos \alpha \quad (30)$$

where D is the drag force, N is the normal force, A is the axial force, and α is the angle of attack.

The pitching moment was also adjusted to be transferred to the aerodynamic center located at quarter chord. The specifications of the balance can be found on pages 56-58 of Subsonic WT manual on D2L [5]. This new reference pitching moment is:

$$P_{mref} = P_m - (A + C)N \quad (31)$$

where P_m is the pitching moment recorded by the balance, A is location of the balance center which is given to be 1.1405", C is the distance from the end of the balance to the reference point (the aerodynamic center/quarter chord), and N is the normal force. It was measured that C in Equation 30 was 0.0175 m.

The lift, drag, and pitching moment are then nondimensionalized into their corresponding coefficients by:

$$C_L = \frac{L}{qS} \quad (32)$$

where C_L is the lift coefficient, L is the lift, Q is the dynamic pressure, and S is the wing area. The coefficient of moment is found by:

$$C_M = \frac{M}{QSc} \quad (33)$$

where M is the reference pitching moment, Q is the dynamic pressure, S is the wing area, and c is the mean aerodynamic chord. The drag coefficient is defined in Equation 10.

The lift slope from A5 for all 4 cases is found in Figure 13. It was found that the case with no slat or flap had the lowest overall lift and stalled at 12° . The slat cases created more lift at high angles of attack, and the flap shifts the lift slope up and stalls around 8° .

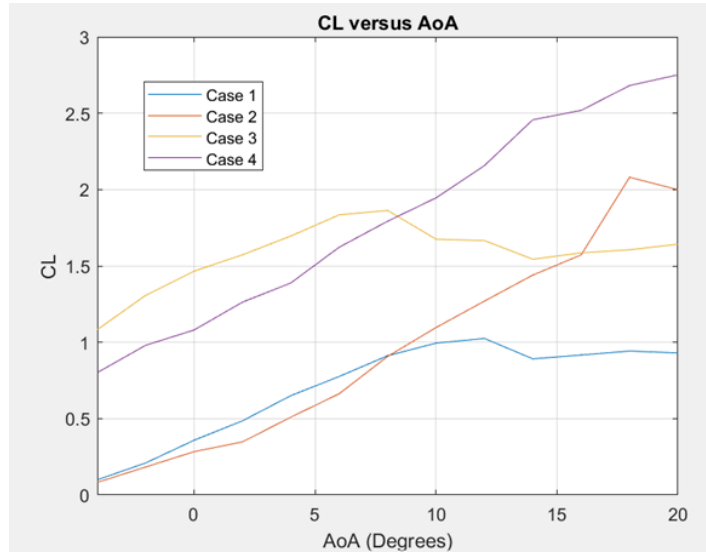


Figure (13) shows the C_L vs α for A5.

The drag as a function of angle of attack can be seen in Figure 13. It is found that the flap cases had an increase in drag. The magnitude of drag also increased more at the stall points defined in the lift slope chart in Figure 14.

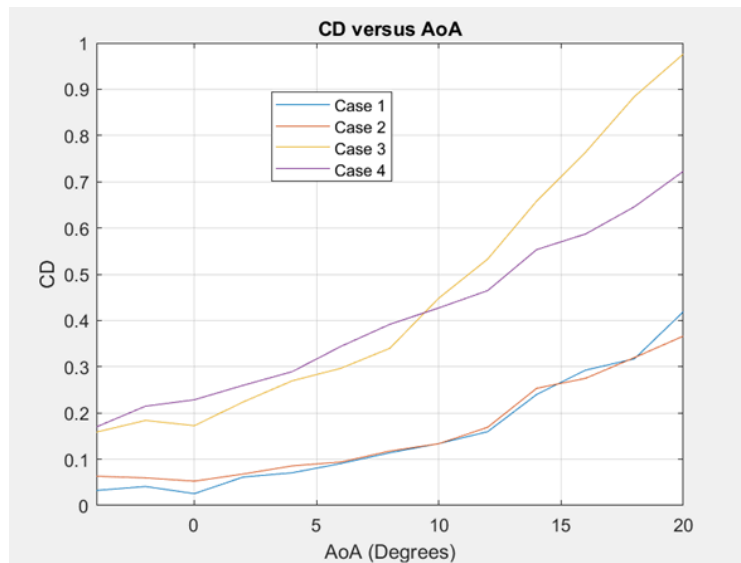


Figure (14) shows the C_D vs α for A5.

The transferred pitching moment as a function of the angle of attack can be found in Figure 15. The distance for C in Equation 31, defined above, had to be adjusted to produce the correct trends on the graph, which is further explained in the Discussion section. This new distance was defined as 0.012m. The flap caused the moment to increase in magnitude. The slat allowed the moment to remain stable, and it had an insignificant effect at low angles of attack.

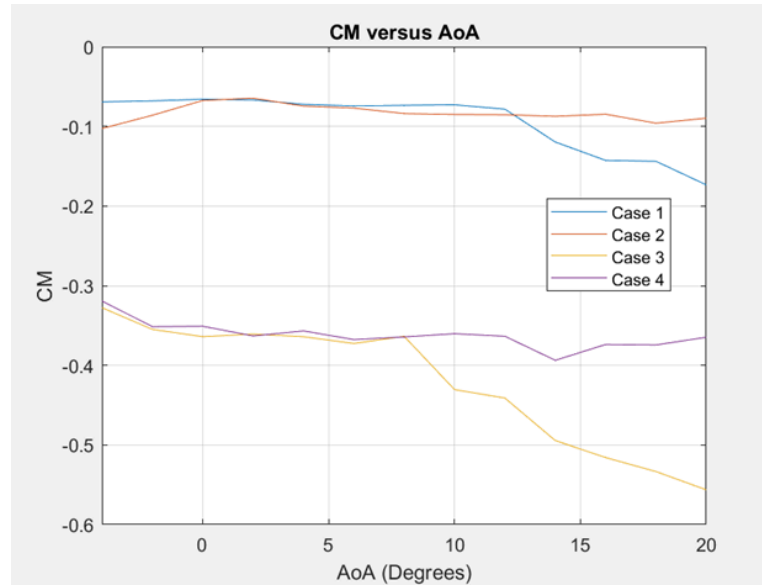


Figure (15) shows the C_M vs α for A5.

The drag polar is shown in Figure 16. The addition of a slat created a higher L/D compared to their respective cases. Adding a flap allowed more lift compared to the drag produced initially, and it caused additional drag after stall.

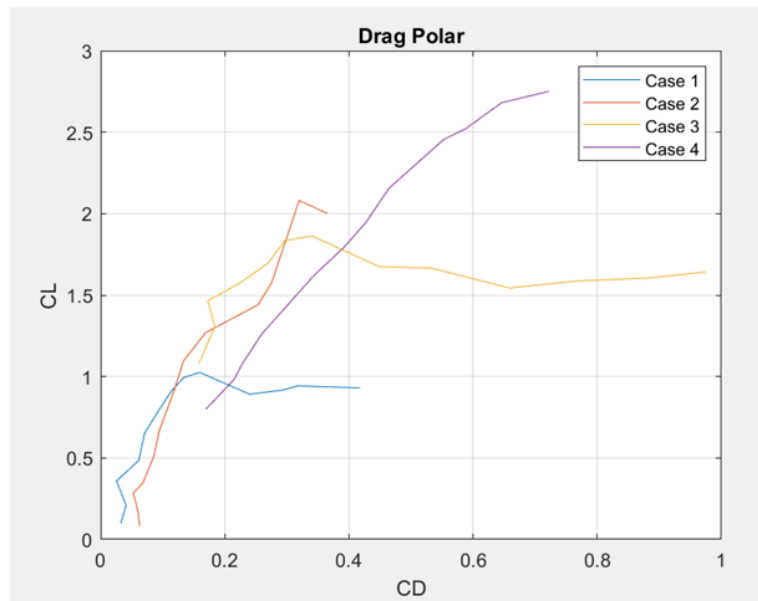


Figure (16) shows the drag polar for A5.

DISCUSSION

The pitot-static tube pressure and velocity readings are fitted with error bars that include the 0.08% of reading sensor accuracy, and a 95% confidence interval with a sample size of 200,000 points. The AEROLAB pressure and velocity readings are very close to the pitot-static tube measurements. This is shown by the slope of the fitted curves being nearly 1. This does not mean that the AEROLAB sensors are faulty or inaccurate. The cause of the pressure difference between the two sensors is a combination of two factors. Firstly, the two sensors are at different positions in the wind tunnel. The AEROLAB sensor is upstream of the test section, where the pitot-static tube was mounted. Most importantly, however, is the existence of the screen at the wind tunnel inlet. The screen is meant to stabilize the flow. However, this is not done to the ideal, theoretical levels of perfectly laminar flow. This can be seen in Figure 5, where the turbulence intensity at all experimental fan speed settings are shown to be exceedingly low, below 0.01. However the turbulence intensity is not 0 either, exemplifying that there is some turbulence occurring in the flow.

One issue however is that the velocity measurements from the pitot-static tube used an incorrect value for the density of air. Using the correct value of 1.08 kg/m^3 , the corrected velocity calibration curve becomes $y = 1.0572x - 0.1479$, the corrected velocity versus fan speed curve becomes $y = 0.6019x - 1.1989$, the anemometer calibration curve becomes $y = 7.206x^4 - 26.555x^3 + 37.799x^2 - 25.967x + 7.5556$. These changes, and the error of using the sea level value for density of air, does not impact any experimental results in this report, as all experiments utilized the pressure calibration curve, which was not impacted by this error.

The data obtained from Experiment 2 yields a pressure distribution and drag coefficients which are in agreement with accepted results from similar experiments on circular cylinders. For low Reynolds numbers (between 50k and 150k), the pressure profile and drag coefficient hardly change at all, with drag coefficients near constant just above $C_D=1$. Only after the Reynolds number surpasses about 500k, or is at least simulated to do so, is there a significant difference in the flow behavior. For after the Reynolds number surpasses 500k, the flow becomes energized as it transitions from laminar to turbulent, delaying separation and decreasing drag (see Figure (7)), in this experiment, cutting drag in half. This behavior was expected by prior knowledge and reinforced during this lab.

Inaccuracies arise from the resolution of the pressure tap locations on the cylinder, as well as the method of using pressure taps to measure drag as a whole. With taps located every 15° , particular locations of significance are unlikely to be accurately captured. This is why the locations of separation, max velocity, and pressure matching are all rough estimates. The data must be interpolated to acquire these values, and the confidence decreases significantly for items close to or after the point of separation. However a much more accurate picture can be painted, even without the addition of more pressure taps on the cylinder. Thanks to its infinite symmetry along its main axis, the cylinder can be rotated just 1° or 2° at a time to obtain pressure data between the 15° markings, which can then be superimposed on to the original data to increase the resolution. This would increase the confidence of interpolation and more accurately capture particular locations, though will take much longer as each slight rotation adds an extra run that

needs to be completed. The other inaccuracy from this experiment cannot be fixed without entirely changing the methodology employed. While measuring with pressure taps does capture *most* of the drag contribution, if a more accurate calculation of total drag is desired, a balance arm must be used, which can measure pressure, skin friction, and 3D effects, though will not provide information on particular locations of significance.

The only cracks in this experiment were the one pressure tap malfunctioning and the asymmetry of the data. For later experiments, the pressure tap associated with $\theta=30^\circ$ should be mended or replaced. To tackle the asymmetry, first ensure that the cylinder is aligned precisely so that the pressure tap at $\theta=0^\circ$ is pointed directly into the freestream and there are no leaks in the walls of the test section, especially near the access panel. It would also be wise to inspect the state of the honeycomb in the inlet and check for any damage which would affect the airflow downstream. After attempting this if nothing changes, the next two options are to 1) try moving the tunnel inlet closer to the center of the room or 2) add another honeycomb structure to straighten the flow in the diffuser just before the fan. The latter option would mean that the tunnel needs to be recalibrated yet again, however this may be worth it if all else fails.

Inspecting the pressure distributions on the Clark Y-14 airfoil from $\alpha = -4^\circ$ to 20° in Experiment 3, it is noted that the stagnation point appears to move towards the lower surface of the airfoil at higher α , when the freestream flow is impinging more on the lower surface of the airfoil, as expected. The flow separation point is near the back of the airfoil initially, but moves forward at higher α , and at $\alpha > 12^\circ$, the flow separation point is so far forward that stall occurs, as expected. This can be seen in Fig. 9 in the plot of C_l vs. α and in the drag polar plot.

$C_l = 0$ does not occur at $\alpha = 0^\circ$, but instead around $\alpha = -4^\circ$, because the Clark Y-14 airfoil has some camber, allowing it to generate lift while pointed straight into an airflow. C_d (minus skin friction drag, accounted for in Experiment A4) is minimized from $-4^\circ < \alpha < 4^\circ$, and increases with α beyond those bounds.

The calculated values of C_l and C_d roughly match published values for a Clark Y-14 airfoil at $Re = 100,000$ [4], shown in Figures 17 and 18. They do not match perfectly, suggesting that the accuracy of the data is limited, perhaps in part by its relatively low resolution in x/c and α , or by errors in pressure measurement. Another likely source of error arises from the lack of pressure taps on the back 20% of the airfoil. The pressure distribution there contributes to lift, drag, and pitching moment, but is not accounted for in the results. One could approximate the pressure distribution on that portion of the airfoil by extrapolation, but because the calculated lift and drag are already within expectations, however it was not seen that this additional work was necessary. However, due to the long moment arm ($x/c = 1$) between the back of the airfoil and the leading edge, it is likely that this did materially affect the $C_{M,LE}$ results. The $C_{M,LE}$ results are nonetheless in line with results reported by other teams.

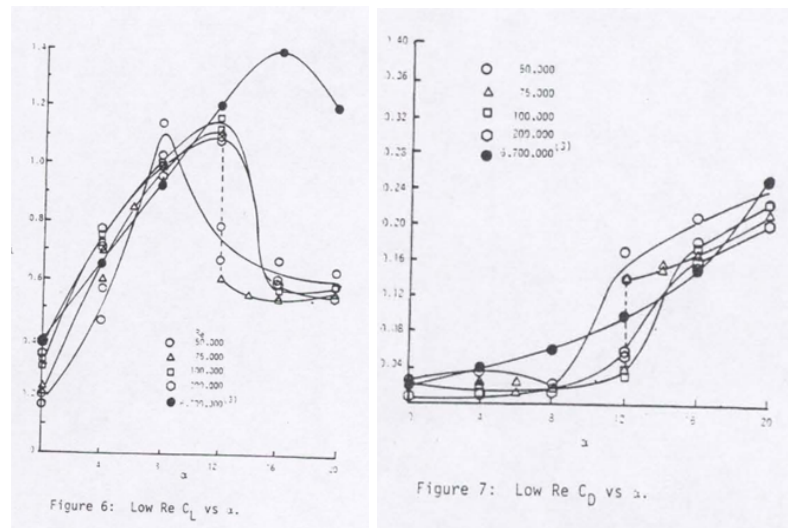
A few things to notice from Figure 11 are that the coefficient of drag is relatively constant in the range of angles of attack from -4° to approximately 8° with the exception of the 0° angle of attack. This discrepancy at 0° is likely an error as it is inconsistent with the rest of the readings. Given that an offset not quite at zero should still result in data that is closer to the 2° and -2° readings, it is unlikely that the error has to do with the airfoil not fully being aligned with the intended angle of attack, but is rather most likely instrumentation error. Ideally, to combat this

another reading at 0° angle of attack should be performed, but this error was not caught until data processing had been completed.

Another thing of note regarding this figure is that after this consistent envelope, around 10° angle of attack the drag coefficient increases very quickly from this point onwards. This suggests that the flow has separated from the airfoil at this angle of attack, which suggests that this increase in drag is related to an increase in pressure drag on the system.

In Figure 12 it can be seen that the general trend between A3 and A4 are very similar, but what is unexpected is that typically lower overall values of drag are shown in the A4 experiment, despite the fact that this portion of the experiment took into account both the surface drag of the airfoil, and the pressure drag of the airfoil, which would lead to conclusion that the overall drag should be larger in the experiment that considers both.

The lift slope in Figure 13 shows that the addition of a slat and a flap in Experiment 5 has a significant effect on the lift. Case 2 shows a continuation of lift after the stall in Case 1, which implies that the addition of a slat aids in creating lift at high angles of attack and delays stall. Case 3 has a slope that is shifted upwards from Case 1, which shows that the addition of a flap improves the lift for low angles of attack. However, it does stall sooner than Case 1. The slat does not have a significant effect on the drag in Case 2 seen in Figure 14. The flap configuration added drag. The flap adds a lot more camber to the airfoil. The shape of the wing with the flap creates separation, which causes more drag, and it stalls sooner. However, adding the slat with the flap in Case 4 shows a decrease in drag, since the slat helps prevent stall at high angles of attack.



Figures (17) and (18) show the lift and drag curves for various Reynolds numbers.

To determine the reliability of the experiment, Case 1 for lift and drag can be compared to previous experiments. Figures 17 and 18 are from previous low Reynolds number data for the Clark Y-14 [4]. This wing has a slightly different aspect ratio than the one analyzed in this report, so the magnitudes of the results will be slightly different. Their wing had an aspect ratio of 5.75, while this experiment has an aspect ratio of 2.82. When comparing lift, it is noted that this experiment and previous low Reynolds number data at an Re of 100,000 both grow linearly until it reaches stall around 12° . The maximum lift coefficient on this experiment was around 1, while

Figure 17 shows a maximum lift around 1.1. The coefficient of lift of a wing compared to a 2D airfoil is directly related with the aspect ratio, so it makes sense that this experiment would have a lower $C_{L,max}$. Overall though, they have the same trend. A similar comparison can be made with the drag coefficient. Both Figures 14 and 18 show a minimal increase in drag until stall is reached at 12° . Then the drag increases. The previous low Reynolds number data has a lower maximum C_D of around 0.24 whereas this experiment was around 0.4, which is caused by the larger aspect ratio. This experiment is subject to lots of induced drag due to the small wingspan and also drag from being in an enclosed test section as described in Experiment 4 versus Experiment 3.

The results can also be compared with other experiments in this report. It is found that the stall point for the Clark Y-14 wing section, shown by a decrease in lift and an increase in drag all occurred around 12° , which confirms the likeness in measurement techniques. However the magnitudes of each value are different. Experiment 5 has the highest drag coefficient at 0.4, compared to 0.3 and 0.18 found in A3 and A4, respectively. It makes sense that A5 has the most because it can measure the data directly whereas A3 was not able to account for skin-friction or induced drag. This also shows why A3 recorded higher lifting forces. Experiment 4 should have been closer to experiment 5 in terms of magnitude, of which was explained earlier in this report with comparison to A3. Overall, the experiments did have similar trends and differences make sense according to what each measurement technique was able to capture, so the experiment is deemed reliable.

The pitching moment coefficient trend shown in Figure 15 was adjusted to create an accurate pitching moment for Case 1 in order to effectively compare the other cases. The pitching moment reference in Equation 31 relies on the distance from the aerodynamic center to the end of the balance. In the lab, this distance was measured to be 0.0175 m. However, when this distance was used to transfer the pitching moment to the aerodynamic center, Case 1 had a negative slope on the C_M vs α graph. It is assumed that the quarter chord of the Clark Y-14 is the aerodynamic center. Since the moment about the aerodynamic center does not change with the angle of attack, this assumption is either incorrect or the distance measured in the lab was wrong. For an effective moment comparison, the distance was changed for C in Equation 31 to 0.012 m to have no change in the moment coefficient for Case 1. However, it can be seen that the moment drops in Case 1 for high angles of attack due to stall. The flow detaches and the turbulence makes the wing unstable. Case 2 combats this by delaying stall for high angles of attack, and the moment coefficient continues to stay level. The addition of a flap in Case 3 increases the magnitude of the moment coefficient and becomes more negative. This is due to the camber in the wing changing the lift distribution and the drag changing the flow over the wing. Adding a slat in Case 4 improves Case 3 by delaying stall and the moment can maintain being level.

The drag polar is seen in Figure 16 for CL as a function of CD. In Case 1, there is a significant L/D until the wing stalls and an increased amount of drag is produced. Adding a slat created a much more effective L/D in Case 2 and Case 4, meaning lift and drag are both increased at a steady rate as angle of attack increases. The delayed stall from the slat rids of the plateaued drag from Case 1 and Case 3. Adding a flap in Case 3 creates a higher L/D than Case 1, but it leads to even more drag than Case 1 once a stall is reached.

CONCLUSIONS

This experiment sought to demonstrate the various collection methods of aerodynamic forces such as lift and drag as well as the moment on an airfoil in a subsonic wind tunnel. To accomplish this, the experiments began with a very basic model, and gradually added sufficient new dimensions so as to explore how different assumptions and complexities changed the behavior of the flow. In the process, techniques for performing wind tunnel experiments were developed. It was learned from A1 that the future results of the wind tunnel can be trusted with very little required manipulation of the data due to low turbulence. All the experiments were then calibrated accordingly. From A2, the drag was found across a simplified airfoil shape, in the form of a cylinder, with discrete stagnation pressure measurement points. This brought insight to the uniformity of flow in the tunnel, as well as the reliability of the pressure measurement techniques. It also observed how the drag changed in different types of flow conditions. A3 expanded on this using a Clark Y-14 airfoil rather than a cylinder to get a more accurate shape for the surface drag caused by separation of the flow. Then A4 further developed these findings by also taking into account the drag measured in the wake of the airfoil as a result of flow separation and skin friction drag. A5 compared all of these findings considering the surface drag, pressure drag, and induced drag as a result of having a finite wing. However, experiments 3, 4, and 5 found similar trends to each other and previous data for the aerodynamic forces of the wing model despite having different magnitudes, which can confirm the reliability of the experiment. It was also noted that a slat positively impacted high angles of attack, and a flap positively affected low angles of attack.

Overall, it is discovered that making different assumptions and using various measurement techniques leads to a range of results even when studying the same system. It is important to consider all affects to the flow on a model used in a subsonic wind tunnel as well as evaluating the accuracy of measurement techniques in order to obtain an accurate analysis of the model.

REFERENCES

- [1] MKS Type 390/590 Absolute MKS Type 398 Differential High Accuracy Pressure Transducers, MKS Instruments, Massachusetts, 1994.
- [2] Jørgensen, F., *How to measure turbulence with hot-wire anemometers*, Dantec Dynamics, Denmark, 2002.
- [3] AEROLAB. (2010). Educational Wind Tunnel (EWT) Operational Manual for the University of Arizona.
- [4] Marchman, I. J., and Werme, T. D., “Clark-Y Airfoil Performance at Low Reynolds Numbers,” *22nd Aerospace Sciences Meeting*, American Institute of Aeronautics and Astronautics, 1984. <https://doi.org/10.2514/6.1984-52>
- [5] Fox, Robert W., and Alan T McDonald. “Fox and McDonald’s Introduction to Fluid Mechanics”. 8th ed., John Wiley & Sons, Inc, 2020.

APPENDICES

A1 Data Sheets

Fan Speed (%)	Pitot-Static Tube Pressure (mBar)	AEROLAB Pressure (mBar)	Anemometer (Volts)	AEROLAB speed (m/s)	Measured velocity (m/s)
0	0.000	0	1.413	0	0.13
5.0	0.024	0.02	1.680	2	2.098
6.5	0.042	0.05	1.729	2.8	2.79
8.3	0.076	0.08	1.786	3.7	3.76
10.8	0.139	0.15	1.847	5	5.07
13.9	0.243	0.27	1.910	6.6	6.71
18.0	0.434	0.48	1.981	8.8	8.97
23.2	0.770	0.83	2.056	11.6	11.94
30.0	1.390	1.49	2.142	15.3	16.05
38.7	2.704	2.77	2.246	21.3	22.38
50.0	4.835	4.97	2.344	28.3	29.92

Fan Speed	u'	u(bar)	TI
5.00	0.01753	1.90859	0.009
6.46	0.01912	2.55085	0.007
8.34	0.02090	3.44740	0.006
10.77	0.02784	4.63104	0.006
13.91	0.02985	6.13694	0.005
17.97	0.03285	8.20931	0.004
23.21	0.04962	10.89475	0.005
29.97	0.07235	14.66598	0.005
38.71	0.07625	20.47301	0.004
50.00	0.15988	27.34452	0.006

A2 Data Sheets

Pressure Tap Location	Readings (Cp)				Cp converted to Pressure (mbar)				Pressure converted to Velocity (m/s)				Pressure Converted to 2D Drag per dx			
	Re = 50k	Re = 100k	Re = 150k	Tripped	Re = 50k	Re = 100k	Re = 150k	Tripped	Re = 50k	Re = 100k	Re = 150k	Tripped	Re = 50k	Re = 100k	Re = 150k	Tripped
0	0.530827667	0.969335	0.994488	0.991834	921.4433832	922.5306471	924.4018077	924.3929961	0	0	0	0	1225.465233	1226.91123	1229.399763	1229.388044
15	0.824424333	0.7960565	0.834735333	0.83455175	921.4041309	922.2746638	923.8714115	923.870802	2.701857599	6.899788625	9.931850004	9.854757695	1183.658093	1184.776401	1186.827622	1186.826839
30	0.447511	0.43481025	0.444659633	0.424954875	921.2658872	921.7416076	922.5761527	922.5108961	5.738385357	12.11577126	18.42635967	18.70963236	1061.078669	1061.627507	1062.588705	1062.513545
45	0.070597667	0.07564	0.054484333	0.015358	921.1260435	921.2089531	921.2089531	921.1509902	7.682315364	15.68055564	24.05189878	24.55482711	866.258347	866.3139382	866.3819699	866.2580771
60	-0.395658	-0.32265575	-0.472831333	-0.59122225	920.9540414	920.6235929	919.5301489	919.1370782	9.539730807	18.83265295	30.10013294	31.2647001	612.4072187	612.1874803	611.4603723	611.1989919
75	-0.65480667	-0.536836	-0.818294333	-1.072639	920.8584877	920.3078429	918.3831744	917.5387226	10.42963485	20.33202297	33.45637812	35.70349224	316.9724122	316.7828725	316.1203746	315.8297025
90	-0.527235333	-0.570352	-0.744576	-1.035753	920.9050024	920.2583865	918.6279272	917.6611881	10.00168066	20.55696751	32.76905191	35.38309699	7.5025E-14	7.49723E-14	7.48395E-14	7.47607E-14
105	-0.547324333	-0.676979	-0.715883	-0.6959555	920.880916	920.1010474	918.7231911	918.7893525	10.07034587	21.25677379	32.49759754	32.28235687	-316.960444	-316.7116906	-316.2374131	-316.2601668
120	-0.491968	-0.75057725	-0.635085	-0.212031	920.9185126	919.9924455	918.9914491	920.3960342	9.879980923	21.72666358	31.72071763	27.26433994	-612.3835931	-611.767859	-611.1021529	-612.0361604
135	-0.914449333	-1.21148025	-1.016082667	-0.40174975	920.7626588	919.3123354	917.7264957	919.7661474	11.25163469	24.46493333	35.2343095	29.33409071	-865.8946163	-864.5307173	-863.0393775	-864.9574868
150	-0.947753	-1.20730375	-1.092901667	-0.4094245	920.7503731	919.3184982	917.4714483	919.7406664	11.35271573	24.44149772	35.90110851	29.41475422	-1060.48584	-1058.83666	-1056.709297	-1059.322898
165	-0.832941	-0.948812	-0.795634667	-0.22942	920.7927273	919.698464	918.4584069	920.3681818	11.0003284	22.95046104	33.24661924	27.35916929	-1182.87267	-1181.46594	-1179.873945	-1182.327288
180	-1.234555	-1.191607667	-0.49366775	0.0445715	920.5445715	918.9975224	917.1769348	919.4608697	12.18855348	25.63359205	36.65600119	30.28603298	-1224.402861	-1222.212383	-1219.791109	-1222.828674
195	-0.677409	-0.8896075	-0.697065667	-0.14387595	920.8501032	919.7867707	918.7856666	920.622037	10.50412349	22.58979317	32.31833544	26.48137527	-1182.946376	-1181.580393	-1180.294351	-1182.653739
210	-0.856779667	-1.16758775	-0.951958333	-0.34039325	920.7839332	919.3771033	917.939354	919.9698576	11.07441777	24.21750601	34.66788209	28.68106344	-1060.524494	-1058.904159	-1057.248261	-1059.568872
225	-0.389604667	-0.526307	-0.416380333	-0.02478475	920.9562745	920.3237395	919.7175723	921.017712	9.517938938	20.26084148	29.51544509	25.05446604	-866.0766945	-865.4815135	-864.9118062	-866.1344709
240	-0.463303333	-0.5098075	-0.568348333	-0.244964	920.929087	920.3474706	919.2130221	920.286693	9.779949928	20.14997033	31.06439097	27.63474624	-612.3906248	-612.0036671	-611.2494924	-611.9634518
255	-0.610175	-0.713794	-0.690843667	-0.8163385	920.8749059	920.046723	918.8063243	918.3896679	10.28221153	21.49310419	32.25884281	33.41381192	-316.9780636	-316.6929914	-316.2660288	-316.1226098
270	-0.855637667	-0.8539315	-0.831848667	-1.27381395	920.7843545	919.8399356	918.3381725	916.8707816	11.0708798	22.36987466	33.58122333	37.40269015	-2.25045E-13	-2.24815E-13	-2.24448E-13	-2.24089E-13
285	-1.274796	-1.33776125	-1.283061	-1.752753	920.6297266	919.1229947	916.8409988	915.2806706	12.30129685	25.16322922	37.50075043	41.16656163	316.8936694	316.3760638	315.5892264	315.0244893
300	-0.822263	-1.1168425	-1.063758	-1.256151	920.796664	919.4532783	917.5681752	916.9294429	10.9697941	23.92711336	35.64969256	37.25665391	612.302569	611.4085907	610.1557178	609.7309797
315	-0.040659667	-0.13525125	-0.138087333	-0.1722125	921.0850039	920.9004228	920.6415351	920.5282359	8.163969972	17.41220093	26.44476081	26.80965705	866.1977529	866.0241709	865.7807103	865.6741626
330	0.371904	0.4581905	0.452372333	0.42409725	921.2371957	921.7761076	922.601925	922.5080487	6.192429756	11.84597992	18.29582817	18.72317933	1061.046544	1061.667243	1062.618399	1062.510265
345	0.918857333	0.974379	0.956136667	0.94057625	921.4389673	923.5377972	924.2144771	924.2228148	0.966229011	#NUM!	4.86627141	5.625802395	1183.702845	1185.114429	1187.34541	1187.279043
360	0.530827667	0.969335	0.994488	0.991834	921.4433832	922.5306471	924.4018077	924.3929961	0	0	0	0				

Total Drag per meter span (N/m)			
Smooth Cylinder			Tripped
Re = 50k	Re = 100k	Re = 150k	Re = 150k
4.019477	19.00082	37.54503	18.06993
Cd			
1.072423	1.267386	1.113029	0.535686

0	0.05	0.1	0.2	0.3	0.4	0.5	0.6	0.7	0.8	0.05	0.1	0.2	0.3	0.4	0.5	0.6	0.7	0.8
0	0	0	0	0	0	0	0	0	0	0	0	0	0	0	0	0	0	0
0.64141	0.52091	0.25223	-0.35623	-0.39706	-0.394196	-0.336682	-0.240263	-0.258449	-0.220239	-1.06971	-1.05912	-0.37456	-0.226259	-0.163526	-0.09912	-0.10962	-0.04374	0
0	0.05	0.1	0.2	0.3	0.4	0.5	0.6	0.7	0.8	0.05	0.1	0.2	0.3	0.4	0.5	0.6	0.7	0.8
0.637547	0.522032	0.252223	-0.365934	-0.398992	-0.38067	-0.333009	-0.228348	-0.270118	-0.208733	-1.063886	-1.048286	-0.354931	-0.230127	-0.167418	-0.110487	-0.067664	-0.061236	0.035062
0	0.05	0.1	0.2	0.3	0.4	0.5	0.6	0.7	0.8	0.05	0.1	0.2	0.3	0.4	0.5	0.6	0.7	0.8
0.649138	0.537567	0.253283	-0.364008	-0.422235	-0.399993	-0.333009	-0.244233	-0.264288	-0.218396	-1.0633	-1.065865	-0.362774	-0.226259	-0.161578	-0.112425	-0.033832	-0.026444	-0.052414
0	0	0	0	0	0	0	0	0	0	0	0	0	0	0	0	0	0	0
0.624023	0.536706	0.227164	-0.36796	-0.38589	-0.390332	-0.321993	-0.244565	-0.206733	-0.163686	-1.050253	-0.374564	-0.226259	-0.161578	-0.109103	-0.056206	-0.034992	0.006766	0
0	0.05	0.1	0.2	0.3	0.4	0.5	0.6	0.7	0.8	0.05	0.1	0.2	0.3	0.4	0.5	0.6	0.7	0.8
0.643342	0.539498	0.013582	-0.378415	-0.414587	-0.384535	-0.330009	-0.256219	-0.264288	-0.208733	-1.079417	-1.065987	-0.35297	-0.233995	-0.171312	-0.098857	-0.050748	0.006736	0.017531

Pressure on airfoil surface at $\alpha = -4$

Average Pressure Coefficient

x/c

Top surface Bottom surface

C. N					C. A						
x/c	y/c.u	y/l.c	Cp.l-Cp.u	trapez. area	x/c	y/c.u	y/l.c	dy.u/dx	dy.l/dx	(Cp.u + dy.u/dx)-(Cp.l + dy.l/dx)	trapez. area
										0.639092	
0.05	0.0442753	-0.0260452	-1.662106	-0.0400653	0.05	0.0442753	-0.0260452	0.48144	-0.13933	0.11571909	0.16877028
0.1	0.0293981	-0.0293786	-1.037758	-0.0603434	0.1	0.0293981	-0.0293786	0.39474	-0.07598	0.06649691	0.09172487
0.2	0.0326022	-0.0266564	0.0031384	-0.0517813	0.2	0.0326022	-0.0266564	0.126865	0.0226125	-0.03840955	-0.0042616
0.3	0.0906804	-0.0263079	0.1766092	0.00898738	0.3	0.0906804	-0.0263079	0.296025	0.0378275	-0.00354366	-0.00287485
0.4	0.0911712	-0.0226341	0.224863	0.02007361	0.4	0.0911712	-0.0226341	-0.0238875	0.03841	0.01532549	0.00598585
0.5	0.0858772	-0.0189619	0.2302776	0.02275703	0.5	0.0858772	-0.0189619	-0.0785675	0.03681	0.02976654	0.0022546
0.6	0.0757633	-0.0152893	0.178761	0.02045193	0.6	0.0757633	-0.0152893	-0.12349	0.0367025	0.00327448	0.00316095
0.7	0.0614239	-0.0116169	0.214912	0.01968365	0.7	0.0614239	-0.0116169	-0.16061	0.036373	0.00343934	0.00379332
0.8	0.0436336	-0.0079443	0.2174788	0.01846429	0.8	0.0436336	-0.0079443	-0.19009	0.036725	0.00402058	0.00419573
C. N = -0.0444331					C. A = 0.0281983						

x	y	yL	x/c	y/c	y/cL	C _M E _h		C _{pl}	dy/dx _h	dy/dx _L	trap area ₁	trap area ₂	trap area ₃
						(C _{pu} -C _{pl})/C _{pl}	C _{pl}						
0.00404	0.0039045	-0.002318	0.04	0.04427	-0.023650	0.0071316	0.02395	-1.702398	0.4814	-0.130	1.567670	2.236867	7.205165
0.0089	0.0050693	-0.022147	0.1	0.026991	-0.027582	0.0025450	0.055395	-1.616902	0.3074	-0.39395	3.63450E	2.152554E	9.52177E
0.0187	0.0074689	-0.022440	0.2	0.038920	-0.029656	-5.588E-5	-3.870804	-3.63951	0.128665	0.021250	4.08917E	-1.72193E	3.67127E
0.0276	0.0080756	-0.026242	0.3	0.0396804	-0.026369	0.0047155	-0.444456	-2.278064	0.0296025	0.0327825	-2.1232E	-1.97781E	-1.86479E
0.0346	0.00811424	-0.020144	0.4	0.019711	-0.022341	-0.0080051	-0.389456	-1.050282	-0.0238875	0.0361	-5.6607E	-9.36091E	-1.43867E
0.0455	0.00764307	-0.016876	0.5	0.058872	-0.018919	-0.0102474	-0.331604	-0.111928	-0.078575	0.03681	-8.12240E	-1.22070E	-0.18917E
0.0534	0.00674293	-0.013607	0.6	0.0797833	-0.013393	-0.013393	-0.294208	-0.064208	-0.12349	0.037025	-8.888	-1.78513E	-2.22569E
0.0613	0.0054673	-0.0100339	0.7	0.0614329	-0.011619	-0.013389	-0.260416	-0.054896	-0.16061	0.03673	-0.0001026	1.91181E	-2.17347E
0.0722	0.00390564	-0.00707	0.8	0.0438634	-0.0079443	-0.0152919	-0.212948	-0.04789	-0.19009	0.036725	-0.00012763	1.21212E	-7.48057E-9

C _{M,le} =	-0.0473212
c (m) =	0.089
C _{M,c/4} =	-0.0584319

$$\alpha = -2^\circ$$

[illegible]

The figure presents a detailed comparison of pressure coefficient (C_p) distributions on an airfoil surface. It consists of three main components: a data table, a plot, and a summary table.

Data Table: The table lists C_p values for 11 different airfoil sections (1.006551 to 1.022007) across 11 spanwise locations (0 to 10.0000). The values are organized into two columns of 11 rows each, with a final row for the mean and standard deviation.

Plot: The plot shows the pressure coefficient distribution on the airfoil surface. The x-axis represents the spanwise location (0 to 10.0000), and the y-axis represents the pressure coefficient (C_p). The plot includes data for the top surface (blue dots) and the bottom surface (red dots). The pressure coefficient is generally negative on the top surface and positive on the bottom surface.

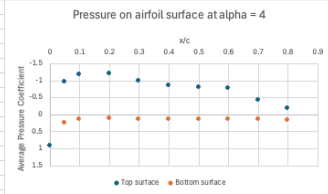
Summary Table: The table provides a summary of the pressure coefficient distribution, including the mean and standard deviation for each airfoil section. The mean values range from 1.022393 to 1.022007, and the standard deviation values range from 0.01096276 to 0.01195052.

	1.006551	-0.11801	-0.59372	-0.793498	0.716637	-0.61255	-0.516939	-0.46681	-0.53635	-0.415533	-0.318389	-0.253713	-0.119617	-0.05028	-0.003893	0.023324	0.008489	0.07909	0.140306
0	0.05	0.1	0.2	0.3	0.4	0.5	0.6	0.7	0.8	0.9	1.0	1.1	1.2	1.3	1.4	1.5	1.6	1.7	
1.023938	-0.141225	-0.59178	-0.808906	-0.728258	-0.608685	-0.526619	-0.462653	-0.524669	-0.415533	-0.318389	-0.245846	-0.143149	-0.052214	-0.01168	0.023324	0.042447	0.052727	0.09646	
0	0.05	0.1	0.2	0.3	0.4	0.5	0.6	0.7	0.8	0.9	1.0	1.1	1.2	1.3	1.4	1.5	1.6	1.7	
1.022007	-0.127683	-0.59372	-0.818536	-0.7147	-0.613784	-0.511131	-0.482509	-0.53052	-0.409735	-0.310624	-0.259613	-0.1255	-0.067684	-0.009734	0.027211	0.016978	0.070274	0.061359	
0	0.05	0.1	0.2	0.3	0.4	0.5	0.6	0.7	0.8	0.9	1.0	1.1	1.2	1.3	1.4	1.5	1.6	1.7	
1.037462	-0.123814	-0.59372	-0.822388	-0.72051	-0.639603	-0.528556	-0.46861	-0.53635	-0.423264	-0.318389	-0.247813	-0.131383	-0.046412	0.001952	0.03693	0	0.070302	0.070153	
0	0.05	0.1	0.2	0.3	0.4	0.5	0.6	0.7	0.8	0.9	1.0	1.1	1.2	1.3	1.4	1.5	1.6	1.7	
1.022007	-0.119945	-0.576257	-0.801202	-0.703079	-0.626077	-0.509195	-0.476553	-0.516917	-0.4136	-0.308682	-0.241912	-0.1255	-0.040611	-0.007787	0.033043	0.067915	0.07909	0.061384	
Mean	1.022393	-0.1261354	-0.5898394	-0.808906	-0.7166368	-0.6237578	-0.518488	-0.471787	-0.5289654	-0.415533	-0.3148946	-0.2497794	-0.1290298	-0.0514402	-0.0062284	0.0287664	0.0271658	0.0702966	
Stdev	0.01096276	0.00921715	0.00763912	0.01195052	0.00918721	0.01299159	0.00808055	0.0077668	0.00829042	0.00492752	0.00483391	0.00695355	0.00892201	0.01010396	0.00540397	0.00605377	0.02776962	0.01076266	

[illegible]

	0	0.05	0.1	0.2	0.3	0.4	0.5	0.6	0.7	0.8	0.05	0.1	0.2	0.3	0.4	0.5	0.6	0.7	0.8
	0	0	0	0	0	0	0	0	0	0	0	0	0	0	0	0	0	0	0
	0	0.05	0.1	0.2	0.3	0.4	0.5	0.6	0.7	0.8	0.05	0.1	0.2	0.3	0.4	0.5	0.6	0.7	0.8
0.944728	-0.96942	-1.197141	-1.211433	-1.011039	-0.858124	-0.822843	-0.800211	-0.427275	-0.191338	0.247282	0.137947	0.123906	0.137624	0.132741	0.147748	0.118851	0.105454	0.157844	
	0	0.05	0.1	0.2	0.3	0.4	0.5	0.6	0.7	0.8	0.05	0.1	0.2	0.3	0.4	0.5	0.6	0.7	0.8
0.923476	-0.948135	-1.164156	-1.190247	-0.961986	-0.858124	-0.797674	-0.784326	-0.429217	-0.170079	0.239494	0.139917	0.119973	0.127932	0.126885	0.128308	0.127374	0.131817	0.157844	
	0	0.05	0.1	0.2	0.3	0.4	0.5	0.6	0.7	0.8	0.05	0.1	0.2	0.3	0.4	0.5	0.6	0.7	0.8
0.938932	-0.96168	-1.19326	-1.207581	-1.02266	-0.861989	-0.818971	-0.774398	-0.429217	-0.18554	0.243388	0.139917	0.125873	0.131809	0.124933	0.138028	0.144319	0.149393	0.184151	
	0	0.05	0.1	0.2	0.3	0.4	0.5	0.6	0.7	0.8	0.05	0.1	0.2	0.3	0.4	0.5	0.6	0.7	0.8
0.931204	-0.982964	-1.19132	-1.219136	-1.009102	-0.86972	-0.817035	-0.790283	-0.431159	-0.195204	0.24923	0.139917	0.13374	0.135686	0.121029	0.141916	0.178276	0.123029	0.184151	
	0	0.05	0.1	0.2	0.3	0.4	0.5	0.6	0.7	0.8	0.05	0.1	0.2	0.3	0.4	0.5	0.6	0.7	0.8
0.92734	-0.94233	-1.179678	-1.197951	-0.989733	-0.84846	-0.784121	-0.78234	-0.45058	-0.166213	0.231706	0.132035	0.110139	0.122117	0.138598	0.130252	0.161298	0.15818	0.131537	
	0	0.05	0.1	0.2	0.3	0.4	0.5	0.6	0.7	0.8	0.05	0.1	0.2	0.3	0.4	0.5	0.6	0.7	0.8
0.915749	-0.93846	-1.175798	-1.163284	-0.978112	-0.831066	-0.789829	-0.76383	-0.417564	-0.179742	0.22197	0.141888	0.121939	0.135686	0.126885	0.128308	0.152808	0.149393	0.157844	

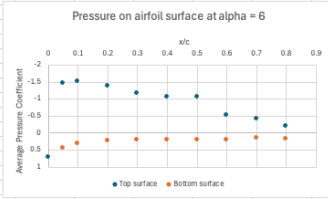
Mean	0.93023817	-0.9571648	-1.1835588	-1.198272	-0.998772	-0.8545805	-0.8050955	-0.7846568	-0.4308353	-0.1813527	0.238845	0.1386035	0.122595	0.131809	0.12851183	0.13576	0.14714867	0.136211	0.1622285
Stddev	0.01049317	0.01724908	0.01257446	0.01991903	0.01798963	0.01341339	0.01658364	0.00951591	0.01080739	0.01155854	0.01035203	0.0034508	0.00773476	0.0058795	0.00622432	0.0081013	0.02191936	0.01984557	0.01980319



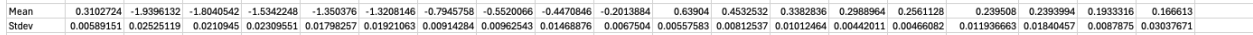
C, N					C, A					
x/c	y/c,u	y/c,l	Cp,l-Cp,u	trapez. area	x/c	y/c,u	y/c,l	dy,u/dx	dy,l/dx	(Cp,u * dy,u)/trapez. area
0	0	0	0	0	0	0	0	10000	10000	0.93023817
0.05	0.0442753	-0.0260452	1.19609083	0.2990025	0.05	0.0442753	-0.0260452	0.48144	-0.13033	-0.429868
0.1	0.0629981	-0.0293786	1.3221623	0.0629454	0.1	0.0629981	-0.0293786	0.30474	-0.03795	-0.355466
0.2	0.0839202	-0.0296656	1.320687	0.13215147	0.2	0.0839202	-0.0296656	0.126865	0.0226125	-0.154791
0.3	0.0906804	-0.0263079	1.130581	0.1225724	0.3	0.0906804	-0.0263079	0.0296025	0.0378275	-0.0345522
0.4	0.0911712	-0.0226341	0.98309233	0.10568367	0.4	0.0911712	-0.0226341	-0.0238875	0.03641	0.01573468
0.5	0.0588772	-0.0189619	0.9430555	0.09619739	0.5	0.0588772	-0.0189619	-0.0785675	0.03681	0.05825702
0.6	0.0757633	-0.0152893	0.9318055	0.09363305	0.6	0.0757633	-0.0152893	-0.12349	0.03625	0.01949655
0.7	0.0614329	-0.0116169	0.56704633	0.07484259	0.7	0.0614329	-0.0116169	-0.16061	0.03673	0.06419343
0.8	0.0438836	-0.0079443	0.34588117	0.04553138	0.8	0.0438836	-0.0079443	-0.19009	0.036725	0.02851549
C, N =	0.76356649				C, A =	-0.0194289				

[illegible]

$$\alpha = 6^\circ$$

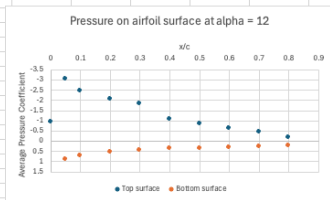


0	0.05	0.1	0.2	0.3	0.4	0.5	0.6	0.7	0.8	0.05	0.1	0.2	0.3	0.4	0.5	0.6	0.7	0.8
0	0.05	0.1	0.2	0.3	0.4	0.5	0.6	0.7	0.8	0.05	0.1	0.2	0.3	0.4	0.5	0.6	0.7	0.8
0.31877	-1.93499	-1.81220	-1.53309	-1.35102	-1.13353	-0.78999	-0.55002	-0.44218	-0.19175	0.63661	0.45328	0.33621	0.29809	0.25371	0.23520	0.22912	0.20219	0.14007
0	0.05	0.1	0.2	0.3	0.4	0.5	0.6	0.7	0.8	0.05	0.1	0.2	0.3	0.4	0.5	0.6	0.7	0.8
0.309113	-1.962059	-1.831606	-1.54877	-1.36161	-1.1347099	-0.787993	-0.559949	-0.452523	-0.210665	0.646439	0.463107	0.33435	0.306262	0.259627	0.237175	0.26317	0.184544	0.173582
0	0.05	0.1	0.2	0.3	0.4	0.5	0.6	0.7	0.8	0.05	0.1	0.2	0.3	0.4	0.5	0.6	0.7	0.8
0.303318	-1.902676	-1.773398	-1.49455	-1.318999	-1.296849	-0.787993	-0.536122	-0.435043	-0.201002	0.532809	0.447341	0.324516	0.29657	0.249866	0.231343	0.25468	0.193532	0.159292
0	0.05	0.1	0.2	0.3	0.4	0.5	0.6	0.7	0.8	0.05	0.1	0.2	0.3	0.4	0.5	0.6	0.7	0.8
0.312977	-1.963994	-1.805651	-1.546551	-1.36161	-1.132131	-0.80929	-0.555978	-0.450343	-0.204867	0.634756	0.4434	0.361451	0.298509	0.257222	0.260504	0.229212	0.184544	0.122768
0	0.05	0.1	0.2	0.3	0.4	0.5	0.6	0.7	0.8	0.05	0.1	0.2	0.3	0.4	0.5	0.6	0.7	0.8
0.307181	-1.963994	-1.802502	-1.548477	-1.357736	-1.136176	-0.797674	-0.557963	-0.470002	-0.193271	0.642545	0.459165	0.350084	0.294632	0.261579	0.233287	0.220723	0.184544	0.119292

[illegible]

[illegible]

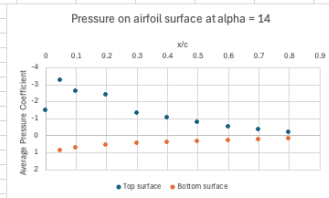
	0	0.05	0.1	0.2	0.3	0.4	0.5	0.6	0.7	0.8	0.05	0.1	0.2	0.3	0.4	0.5	0.6	0.7	0.8
	0	0	0	0	0	0	0	0	0	0	0	0	0	0	0	0	0	0	0
	0	0.05	0.1	0.2	0.3	0.4	0.5	0.6	0.7	0.8	0.05	0.1	0.2	0.3	0.4	0.5	0.6	0.7	0.8
-0.951161	-0.328227	-2.45831	-2.08395	-1.840013	-1.057193	-0.857693	-0.623489	-0.462233	-0.191338	0.885933	0.697616	0.505459	0.443886	0.372847	0.324658	0.314106	0.219695	0.254304	
	0	0.05	0.1	0.2	0.3	0.4	0.5	0.6	0.7	0.8	0.05	0.1	0.2	0.3	0.4	0.5	0.6	0.7	0.8
-0.985889	-0.380471	-2.512637	-2.093525	-1.886498	-1.074543	-0.871245	-0.613561	-0.454465	-0.187473	0.90151	0.677909	0.52906	0.443886	0.372847	0.338266	0.314106	0.219695	0.19292	
	0	0.05	0.1	0.2	0.3	0.4	0.5	0.6	0.7	0.8	0.05	0.1	0.2	0.3	0.4	0.5	0.6	0.7	0.8
-0.962737	-0.392081	-2.489354	-2.093777	-1.892306	-1.086183	-0.863501	-0.621504	-0.454465	-0.191338	0.885933	0.713382	0.525126	0.440009	0.376751	0.342154	0.280257	0.26374	0.245547	
	0	0.05	0.1	0.2	0.3	0.4	0.5	0.6	0.7	0.8	0.05	0.1	0.2	0.3	0.4	0.5	0.6	0.7	0.8
-0.933797	-2.985658	-2.440848	-2.029968	-1.838076	-1.049462	-0.851884	-0.60959	-0.448638	-0.193271	0.876198	0.67988	0.515293	0.438071	0.357231	0.328546	0.339706	0.272531	0.236777	
	0	0.05	0.1	0.2	0.3	0.4	0.5	0.6	0.7	0.8	0.05	0.1	0.2	0.3	0.4	0.5	0.6	0.7	0.8
-0.974313	-0.324357	-2.452489	-2.070414	-1.851634	-1.068789	-0.84414	-0.611576	-0.45058	-0.193271	0.883986	0.70747	0.521193	0.434194	0.374799	0.328546	0.331213	0.246157	0.18416	
	0	0.05	0.1	0.2	0.3	0.4	0.5	0.6	0.7	0.8	0.05	0.1	0.2	0.3	0.4	0.5	0.6	0.7	0.8
-0.980101	-3.066927	-2.487414	-2.101229	-1.886498	-1.074587	-0.849498	-0.623489	-0.460291	-0.193271	0.895669	0.70747	0.531027	0.441948	0.378703	0.338266	0.322721	0.272531	0.210468	
	0	0.05	0.1	0.2	0.3	0.4	0.5	0.6	0.7	0.8	0.05	0.1	0.2	0.3	0.4	0.5	0.6	0.7	0.8
-0.953275	-2.984304	-2.412215	-2.051552	-1.830686	-1.049462	-0.848177	-0.617656	-0.43099	-0.18171	0.860789	0.662144	0.499657	0.397443	0.363087	0.33049	0.331213	0.281322	0.228007	

[illegible]

Pressure on airfoil surface at alpha = 12		C.N						C.A					
		x/c	y/c,μ	y/c,l	Cp,l - Cp,u	trapez.area		x/c	y/c,μ	y/c,l	dy,u/dx	dy,l/dx	(Cp,u * dy,u)/trapez.area
<p>Average Pressure Coefficient</p> <p>x/c</p> <p>Top surface Bottom surface</p>	0.05	0.0442753	-0.0260452	3.92172043	0.09804301		0.05	0.0442753	-0.0260452	0.48144	10000	-0.963039	
	0.1	0.0629981	-0.0293786	3.15701971	0.1769685		0.1	0.0629981	-0.0293786	0.30474	-0.03795	-0.750829	-0.0518044
	0.2	0.0839202	-0.0296656	2.59353929	0.28752795		0.2	0.0839202	-0.0296656	0.126865	0.026125	-0.275014	-0.0500049
	0.3	0.0906804	-0.0263079	2.29502143	0.24442804		0.3	0.0906804	-0.0263079	0.0296025	0.0378275	-0.0715097	-0.0173262
	0.4	0.0911712	-0.0226341	1.43719914	0.18661103		0.4	0.0911712	-0.0226341	-0.0238875	0.03641	0.01196705	-0.0029771
	0.5	0.0858772	-0.0189619	1.18821269	0.13127077		0.5	0.0858772	-0.0189619	-0.0785675	0.03681	0.0549357	0.00334514
	0.6	0.0757633	-0.0152893	0.93631243	0.10622644		0.6	0.0757633	-0.0152893	-0.12349	0.0367025	0.06451645	0.00597261
	0.7	0.0614329	-0.0116169	0.70533329	0.08208229		0.7	0.0614329	-0.0116169	-0.16061	0.03673	0.06322488	0.00638707
	0.8	0.0438836	-0.0079443	0.41197929	0.05586523		0.8	0.0438836	-0.0079443	-0.19009	0.036725	0.02801909	0.00456222
		C.N =	1.36902365					C.A =	-0.1595988				

[illegible]

	0	0.05	0.1	0.2	0.3	0.4	0.5	0.6	0.7	0.8	0.05	0.1	0.2	0.3	0.4	0.5	0.6	0.7	0.8
	0	0	0	0	0	0	0	0	0	0	0	0	0	0	0	0	0	0	0
	0	0.05	0.1	0.2	0.3	0.4	0.5	0.6	0.7	0.8	0.05	0.1	0.2	0.3	0.4	0.5	0.6	0.7	0.8
-1.477869	-3.320408	-2.689201	-2.413236	-1.328683	-1.093914	-0.778313	-0.516265	-0.380663	-0.201002		0.932664	0.772502	0.578229	0.4749	0.396272	0.347986	0.25478	0.272531	0.228007
	0	0.05	0.1	0.2	0.3	0.4	0.5	0.6	0.7	0.8	0.05	0.1	0.2	0.3	0.4	0.5	0.6	0.7	0.8
-1.472081	-3.219789	-2.599949	-2.405532	-1.29963	-1.049462	-0.76476	-0.516265	-0.367068	-0.193271		0.922928	0.744912	0.554628	0.459393	0.396272	0.34021	0.314228	0.246157	0.236777
	0	0.05	0.1	0.2	0.3	0.4	0.5	0.6	0.7	0.8	0.05	0.1	0.2	0.3	0.4	0.5	0.6	0.7	0.8
-1.450858	-3.200439	-2.588307	-2.409384	-1.297693	-1.061058	-0.737382	-0.478538	-0.349588	-0.177809		0.919034	0.721264	0.546761	0.459393	0.388464	0.332434	0.263272	0.272531	0.236777
	0	0.05	0.1	0.2	0.3	0.4	0.5	0.6	0.7	0.8	0.05	0.1	0.2	0.3	0.4	0.5	0.6	0.7	0.8
-1.365968	-3.154	-2.541741	-2.293826	-1.266704	-1.032068	-0.751207	-0.506337	-0.382605	-0.193271		0.895669	0.729147	0.552661	0.45164	0.386512	0.344098	0.331213	0.246157	0.149082
	0	0.05	0.1	0.2	0.3	0.4	0.5	0.6	0.7	0.8	0.05	0.1	0.2	0.3	0.4	0.5	0.6	0.7	0.8
-1.454999	-3.189451	-2.58105	-2.417556	-1.305696	-1.068789	-0.772655	-0.494522	-0.343627	-0.204907		0.899739	0.717323	0.535066	0.461421	0.374799	0.33049	0.339706	0.254948	0.228007
	0	0.05	0.1	0.2	0.3	0.4	0.5	0.6	0.7	0.8	0.05	0.1	0.2	0.3	0.4	0.5	0.6	0.7	0.8
-1.472367	-3.245576	-2.619863	-2.396367	-1.303758	-1.078453	-0.788147	-0.536229	-0.378573	-0.199108		0.899739	0.711411	0.537033	0.449789	0.372847	0.34021	0.271765	0.254948	0.236777
	0	0.05	0.1	0.2	0.3	0.4	0.5	0.6	0.7	0.8	0.05	0.1	0.2	0.3	0.4	0.5	0.6	0.7	0.8
-1.474296	-3.288154	-2.629566	-2.384809	-1.297946	-1.082318	-0.788147	-0.536229	-0.3611	-0.195242		0.917267	0.721264	0.540968	0.453667	0.368943	0.342154	0.28875	0.219783	0.228007



Pressure on airfoil surface at alpha = 14										C.N					C.A						
										x/c	y/c,μ	y/c,l	Cp,l-Cp,u	trapez.area	x/c	y/c,μ	y/c,l	dy,u/dx	dy,l/dx	(Cp,u * dy,u)/trapez.area	
										0	0	0	0	0	0	0	0	10000	10000	-1.452634	
<p>Average Pressure Coefficient</p> <p>x/c</p> <p>Top surface Bottom surface</p>										0.05	0.0442753	-0.0260452	4.143551	0.10358878	0.05	0.0442753	-0.0260452	0.48144	-0.13033	-0.1306713	-0.7272236
										0.1	0.0629981	-0.0293786	3.33821429	0.18704413	0.1	0.0629981	-0.0293786	0.30474	-0.037595	-0.7670003	-0.0550918
										0.2	0.0839202	-0.0296656	2.938008	0.31381111	0.2	0.0839202	-0.0296656	0.126865	0.0226125	-0.3154608	-0.0541231
										0.3	0.0906804	-0.0263079	1.75861614	0.23483121	0.3	0.0906804	-0.0263079	0.0296025	0.0378275	-0.0558314	-0.185646
										0.4	0.0911712	-0.0226341	1.45002443	0.16043203	0.4	0.0911712	-0.0226341	-0.0238875	0.03641	0.01151674	-0.0022157
										0.5	0.0856772	-0.0189619	1.107799	0.12789117	0.5	0.0856772	-0.0189619	-0.0785675	0.03681	0.0474885	-0.00296626
										0.6	0.075633	-0.0152893	0.80687129	0.09573351	0.6	0.0756333	-0.0152893	-0.12349	0.0367025	0.05241318	0.00501308
										0.7	0.0614329	-0.0116169	0.61861129	0.07127413	0.7	0.0614329	-0.0116169	-0.16061	0.03673	0.04953935	0.00509763
										0.8	0.0438836	-0.0079443	0.41543486	0.05170231	0.8	0.0438836	-0.0079443	-0.19009	0.036725	0.02895944	0.00392494
										C.N = 1.34630838					C.A = -0.1852239						

[illegible]

	0	0.05	0.1	0.2	0.3	0.4	0.5	0.6	0.7	0.8	0.05	0.1	0.2	0.3	0.4	0.5	0.6	0.7	0.8
	0	0	0	0	0	0	0	0	0	0	0	0	0	0	0	0	0	0	0
	0	0.05	0.1	0.2	0.3	0.4	0.5	0.6	0.7	0.8	0.05	0.1	0.2	0.3	0.4	0.5	0.6	0.7	0.8
	0.343889	-1.000574	-0.786653	-0.780168	-0.786517	-0.786613	-0.750999	-0.736818	-0.735973	-0.759703	0.673831	0.476901	0.316712	0.224895	0.171783	0.12442	0.067941	-0.026251	-0.069903
	0	0.05	0.1	0.2	0.3	0.4	0.5	0.6	0.7	0.8	0.05	0.1	0.2	0.3	0.4	0.5	0.6	0.7	0.8
	0.39412	-0.954126	-0.739384	-0.718525	-0.709027	-0.69191	-0.679704	-0.679223	-0.728024	-0.68238	0.638776	0.449312	0.306876	0.221017	0.148358	0.097203	0.076434	-0.043751	-0.096117
	0	0.05	0.1	0.2	0.3	0.4	0.5	0.6	0.7	0.8	0.05	0.1	0.2	0.3	0.4	0.5	0.6	0.7	0.8
	0.388324	-0.901871	-0.673402	-0.674219	-0.683843	-0.670651	-0.673894	-0.689153	-0.737731	-0.709443	0.629038	0.461136	0.308843	0.236527	0.158118	0.104799	0.076434	-0.043751	-0.113592
	0	0.05	0.1	0.2	0.3	0.4	0.5	0.6	0.7	0.8	0.05	0.1	0.2	0.3	0.4	0.5	0.6	0.7	0.8
	0.399916	-0.954126	-0.719977	-0.716598	-0.724525	-0.728632	-0.699069	-0.701069	-0.766852	-0.730707	0.658251	0.453253	0.312778	0.228772	0.154214	0.120532	0.093419	-0.00875	-0.087379
	0	0.05	0.1	0.2	0.3	0.4	0.5	0.6	0.7	0.8	0.05	0.1	0.2	0.3	0.4	0.5	0.6	0.7	0.8
	0.367072	-0.939092	-0.723859	-0.735862	-0.753594	-0.728632	-0.702942	-0.707027	-0.770735	-0.738506	0.666041	0.461136	0.306876	0.222956	0.158118	0.128309	0.067941	-0.0175	-0.157282
	0	0.05	0.1	0.2	0.3	0.4	0.5	0.6	0.7	0.8	0.05	0.1	0.2	0.3	0.4	0.5	0.6	0.7	0.8
	0.397984	-0.925096	-0.694749	-0.703114	-0.703216	-0.693843	-0.675831	-0.673265	-0.7222	-0.661116	0.654356	0.457195	0.302942	0.222956	0.152262	0.110811	0.067941	-0.035001	-0.104854
	0	0.05	0.1	0.2	0.3	0.4	0.5	0.6	0.7	0.8	0.05	0.1	0.2	0.3	0.4	0.5	0.6	0.7	0.8
	0.448215	-0.859294	-0.644292	-0.641471	-0.65091	-0.655189	-0.652593	-0.657377	-0.728024	-0.703644	0.644618	0.4434	0.29106	0.230711	0.158118	0.116643	0.033971	-0.0175	-0.096117
	0	0.05	0.1	0.2	0.3	0.4	0.5	0.6	0.7	0.8	0.05	0.1	0.2	0.3	0.4	0.5	0.6	0.7	0.8
	0.461738	-0.886389	-0.66758	-0.681924	-0.69353	-0.705439	-0.702942	-0.705041	-0.764911	-0.736506	0.640723	0.459165	0.308843	0.230711	0.158118	0.101091	0.093419	-0.0175	-0.104854
Mean	0.40015725	-0.9265473	-0.7037245	-0.7064851	-0.713144	-0.7076136	-0.6925993	-0.6936216	-0.7518063	-0.7150006	0.65070425	0.45768725	0.307122	0.22731813	0.15738613	0.11299838	0.0721875	-0.0262505	-0.1037623
Stdev	0.03881042	0.04434734	0.04093064	0.04212557	0.042055	0.04084813	0.03178585	0.02445652	0.02649243	0.03228771	0.01506523	0.00							

	0	0.05	0.1	0.2	0.3	0.4	0.5	0.6	0.7	0.8	0.9	0.05	0.1	0.2	0.3	0.4	0.5	0.6	0.7	0.8
	0	0	0	0	0	0	0	0	0	0	0	0	0	0	0	0	0	0	0	0
	0	0	0	0	0	0	0	0	0	0	0	0	0	0	0	0	0	0	0	0
0.189332	-0.882518	-0.7879	-0.772462	-0.769802	-0.761488	-0.764909	-0.766678	-0.762111	-0.767866	0.724465	0.526168	0.358022	0.275302	0.191304	0.126364	0.067941	-0.026251	-0.087379	0.7	0.8
0	0	0.05	0.1	0.2	0.3	0.4	0.5	0.6	0.7	0.8	0.9	0	0	0	0	0	0	0	0	0
0.204788	-0.828328	-0.770434	-0.766683	-0.772596	-0.753757	-0.759099	-0.766608	-0.81927	-0.777101	0.734203	0.537992	0.358022	0.259792	0.179991	0.122476	0.093419	-0.00875	-0.087379	0.7	0.8
0	0	0.05	0.1	0.2	0.3	0.4	0.5	0.6	0.7	0.8	0.9	0	0	0	0	0	0	0	0	0
0.142965	-0.843511	-0.768483	-0.782094	-0.776831	-0.782748	-0.776528	-0.778525	-0.848391	-0.794409	0.740405	0.541933	0.363904	0.271424	0.189352	0.134114	0.118897	-0.043751	-0.131068	0.7	0.8
0	0	0.05	0.1	0.2	0.3	0.4	0.5	0.6	0.7	0.8	0.9	0	0	0	0	0	0	0	0	0
0.282066	-0.750914	-0.688927	-0.697335	-0.705153	-0.695776	-0.704878	-0.703055	-0.768794	-0.734573	0.724465	0.512374	0.358022	0.257853	0.181543	0.118598	0.076344	0	-0.087379	0.7	0.8
0	0	0.05	0.1	0.2	0.3	0.4	0.5	0.6	0.7	0.8	0.9	0	0	0	0	0	0	0	0	0
0.208652	-0.795427	-0.739384	-0.751399	-0.74196	-0.728632	-0.731989	-0.726888	-0.795973	-0.730707	0.730308	0.520256	0.361957	0.267547	0.1874	0.130252	0.025478	-0.00875	-0.104854	0.7	0.8
0	0	0.05	0.1	0.2	0.3	0.4	0.5	0.6	0.7	0.8	0.9	0	0	0	0	0	0	0	0	0
0.220243	-0.812846	-0.743265	-0.739714	-0.747772	-0.73443	-0.724243	-0.724902	-0.766852	-0.715242	0.724465	0.526168	0.350154	0.267547	0.179991	0.126364	0.033971	-0.096253	-0.12233	0.7	0.8
0	0	0.05	0.1	0.2	0.3	0.4	0.5	0.6	0.7	0.8	0.9	0	0	0	0	0	0	0	0	0
0.210584	-0.845746	-0.75879	-0.739714	-0.740023	-0.738295	-0.723037	-0.722916	-0.795973	-0.748105	0.722518	0.515434	0.354088	0.261791	0.173735	0.12442	0.101912	-0.0175	-0.148544	0.7	0.8
0	0	0.05	0.1	0.2	0.3	0.4	0.5	0.6	0.7	0.8	0.9	0	0	0	0	0	0	0	0	0
0.264678	-0.78198	-0.714155	-0.72623	-0.716778	-0.71317	-0.718433	-0.734832	-0.8056	-0.751971	0.73615	0.534051	0.358022	0.26560	0.183495	0.12849	0.101913	-0.052501	-0.15728	0.7	0.8
0	0	0.05	0.1	0.2	0.3	0.4	0.5	0.6	0.7	0.8	0.9	0	0	0	0	0	0	0	0	0
0.220243	-0.832199	-0.749087	-0.782094	-0.788454	-0.786546	-0.797829	-0.800771	-0.83316	-0.741993	0.536021	0.371792	0.273363	0.183495	0.128308	0.050956	0.008791	-0.087379	0.7	0.8	
0	0	0.05	0.1	0.2	0.3															

[illegible]

A4 Data Sheets

	q_{aerolab}				
		Re_x:	100000		
	1.86988801	p_∞:	27.5 inHg	93125.69 Pa	
		T:	23 °C	296 K	
In Lab:	1.806731888	ρ:	1.09622 kg/m ³		
		μ:	1.8E-05 m ² /s		
		x:	3.5 in	0.0889 m	
		Calibration Factor:	0.9743 A		
			-0.0151 B		
Rake Distance					
[m]					
0.00635					

AoA	C _d Wake	C _d Surface	Error
-4	0.0248	0.0153	38.26
-2	0.0252	-0.0016	106.41
0	0.0101	-0.0079	178.38
2	0.0197	-0.0029	114.76
4	0.0163	0.0107	34.49
6	0.0234	0.0324	38.84
8	0.0360	0.0639	77.73
10	0.0622	0.1044	67.83
12	0.1107	0.1521	37.41
14	0.1660	0.1812	9.14
16		0.1838	
18		0.2263	
20		0.2705	

AoA		-4					-2					
Rake Position	C _p	Normalized C _p	Inner Equation	Sum	C _{d,tot}		Rake Position	C _p	Normalized C _p	Inner Equation	Sum	C _{d,tot}
1	0.984164	1	0	0.01237939	0.02475878		1	0.971706	1	0	0.012618662	0.025237323
2	0.984222	1.000058933	-2.10479E-06				2	0.973796	1.002150856	-7.68576E-05		
3	0.983482	0.999307026	2.47448E-05				3	0.956337	0.984183488	0.000562624		
4	0.97963	0.995393044	0.000164344				4	0.969253	0.997475574	9.01011E-05		
5	0.982329	0.998135473	6.65592E-05				5	0.955216	0.983029846	0.000603484		
6	0.980796	0.996577806	0.000122116				6	0.970384	0.998639506	4.85725E-05		
7	0.977966	0.993702269	0.000224564				7	0.951044	0.978736367	0.000755335		
8	0.979713	0.99547738	0.000161339				8	0.969018	0.997233731	9.87269E-05		
9	0.933471	0.948491308	0.001815277				9	0.904169	0.930496467	0.00243757		
10	0.937868	0.95295906	0.001659797				10	0.97322	1.001558084	-5.56675E-05		
11	0.680086	0.691029137	0.010018035				11	0.686364	0.706349451	0.009578324		
12	0.980391	0.996166289	0.000136787				12	0.942463	0.969905506	0.001066593		
13	0.982677	0.998489073	5.39413E-05				13	0.97211	1.000415764	-1.48502E-05		
14	0.981179	0.996966969	0.00010824				14	0.96868	0.996885889	0.000111132		
15	0.979728	0.995492621	0.000160796				15	0.969238	0.997460137	9.06517E-05		
16	0.975511	0.991207766	0.000313315				16	0.965066	0.993166657	0.00024363		
17	1.030515	1.047096825	-0.001701381				17	1.021395	1.051135837	-0.001849048		
18	1.010091	1.026344187	-0.00094698				18	1.000651	1.029787816	-0.001071657		

0						2					
Rake Position	C_p	Normalized C_p	Inner Equation	Sum	$C_{d,tot}$	Rake Position	C_p	Normalized C_p	Inner Equation	Sum	$C_{d,tot}$
1	0.967553	1	0	0.005062191	0.010124383	1	0.990393	1	0	0.009851048	0.019702095
2	0.965644	0.998026981	7.04302E-05			2	0.988586	0.998175472	6.51E-05		
3	0.966777	0.999197977	2.86379E-05			3	0.987658	0.99723847	9.86E-05		
4	0.963214	0.995515491	0.000159981			4	0.986048	0.995612853	0.000157		
5	0.965644	0.998026981	7.04302E-05			5	0.988586	0.998175472	6.51E-05		
6	0.978714	1.011535285	-0.000413156			6	1.00162	1.011335904	-0.00041		
7	0.961473	0.993716107	0.000224071			7	0.984414	0.993963003	0.000215		
8	0.9626	0.994880901	0.00018259			8	0.986131	0.995696658	0.000154		
9	0.916367	0.947097472	0.001863704			9	0.924736	0.933706115	0.002327		
10	0.981538	1.014453989	-0.000518066			10	0.987969	0.997552487	8.74E-05		
11	0.920732	0.951608852	0.001706825			11	0.987694	0.997274819	9.73E-05		
12	0.781503	0.807710792	0.00650118			12	0.677726	0.684300071	0.010209		
13	0.965962	0.998355646	5.87028E-05			13	0.987099	0.996674048	0.000119		
14	0.979096	1.011930096	-0.000427338			14	0.989511	0.999109444	3.18E-05		
15	0.965043	0.997405827	9.25889E-05			15	0.986022	0.99558866	0.000157		
16	0.973422	1.006065818	-0.000216964			16	0.97988	0.989385022	0.000378		
17	1.030916	1.065487885	-0.00237594			17	1.049163	1.05934008	-0.00215		
18	1.019578	1.053769664	-0.001945488			18	1.038459	1.048532249	-0.00175		

4						6					
Rake Position	C_p	Normalized C_p	Inner Equation	Sum	$C_{d,tot}$	Rake Position	C_p	Normalized C_p	Inner Equation	Sum	$C_{d,tot}$
1	0.96963	1	0	0.008153179	0.016306358	1	0.965477	1	0	0.01167541	0.023350819
2	0.967729	0.998039458	7E-05			2	0.963558	0.998012381	7.09511E-05		
3	0.968865	0.999211039	2.82E-05			3	0.964689	0.999183823	2.91432E-05		
4	0.965289	0.995523035	0.00016			4	0.961138	0.995505848	0.000160325		
5	0.967729	0.998039458	7E-05			5	0.963558	0.998012381	7.09511E-05		
6	0.982878	1.013662944	-0.00049			6	0.976631	1.011552839	-0.000413786		
7	0.963558	0.993737818	0.000223			7	0.959387	0.993692237	0.000224921		
8	0.966879	0.997162835	0.000101			8	0.9626	0.997020126	0.000106345		
9	0.893354	0.921334942	0.002752			9	0.878708	0.910128361	0.003134151		
10	0.96925	0.999608098	1.4E-05			10	0.96509	0.999599162	1.43142E-05		
11	0.970954	1.001365469	-4.9E-05			11	0.966769	1.001338199	-4.78088E-05		
12	0.811154	0.836560337	0.005577			12	0.914931	0.947646604	0.00184463		
13	0.86239	0.889401112	0.003834			13	0.659475	0.683056147	0.010243997		
14	0.96868	0.999020245	3.5E-05			14	0.96243	0.996844047	0.000112624		
15	0.969238	0.999595722	1.44E-05			15	0.965043	0.999550481	1.60524E-05		
16	0.961077	0.99117911	0.000314			16	0.958987	0.993277934	0.000239669		
17	1.040039	1.072614296	-0.00264			17	1.030916	1.067778932	-0.00246036		
18	1.019578	1.051512433	-0.00186			18	1.010137	1.046256928	-0.001670708		

8						10					
Rake Position	C_p	Normalized C_p	Inner Equation	Sum	$C_{d,tot}$	Rake Position	C_p	Normalized C_p	Inner Equation	Sum	$C_{d,tot}$
1	0.977935	1	0	0.017990335	0.03598067	1	0.992469	1	0	0.031094705	0.062189411
2	0.976072	0.998095	6.80045E-05			2	0.978349	0.985773	0.000506292		
3	0.975129	0.997131	0.000102402			3	0.97532	0.982721	0.000614423		
4	0.973593	0.99556	0.000158394			4	0.973782	0.981171	0.000669262		
5	0.959574	0.981225	0.000667368			5	0.974176	0.981568	0.000655217		
6	0.974549	0.996538	0.00012355			6	0.991208	0.998729	4.5363E-05		
7	0.969815	0.991697	0.000295925			7	0.971901	0.979276	0.00073627		
8	0.975435	0.997444	9.12418E-05			8	0.975631	0.983034	0.000603328		
9	0.878708	0.898534	0.003526876			9	0.90346	0.910316	0.003127787		
10	0.97757	0.999627	1.33286E-05			10	0.992129	0.999657	1.2234E-05		
11	0.979324	1.00142	-5.07444E-05			11	0.993972	1.001514	-5.41064E-05		
12	0.950935	0.972391	0.000979141			12	0.834451	0.840783	0.005439945		
13	0.596064	0.609513	0.012228584			13	0.560242	0.564493	0.013345316		
14	0.889519	0.909589	0.00315248			14	0.791764	0.797772	0.006814916		
15	0.975532	0.997543	8.77038E-05			15	0.973434	0.980821	0.000681664		
16	0.967345	0.989171	0.000385695			16	0.984059	0.991526	0.000301992		
17	1.040039	1.063505	-0.002302953			17	1.021793	1.029547	-0.001062914		
18	1.019578	1.042583	-0.001536661			18	1.029432	1.037243	-0.001342284		

12						14					
Rake Position	C_p	Normalized C_p	Inner Equation	Sum	$C_{d,tot}$	Rake Position	C_p	Normalized C_p	Inner Equation	Sum	$C_{d,tot}$
1	0.967553	1	0	0.055335948	0.110671895	1	0.950943	1	0	0.08301744	0.166034881
2	0.967918	1.00037724	-1.34741E-05			2	0.949144	0.998108194	6.75325E-05		
3	0.964877	0.99723426	9.8708E-05			3	0.94817	0.997083947	0.000104069		
4	0.963401	0.995708762	0.000153094			4	0.94679	0.995632756	0.000155802		
5	0.963746	0.996065332	0.000140385			5	0.947058	0.995914582	0.000145758		
6	0.980796	1.013687106	-0.000490486			6	0.964137	1.013874649	-0.00049723		
7	0.961472	0.993715073	0.000224108			7	0.938531	0.986947693	0.000464623		
8	0.956375	0.988447144	0.000411403			8	0.902886	0.949463848	0.001781465		
9	0.844903	0.873236918	0.004373896			9	0.681778	0.716949386	0.009269947		
10	0.786215	0.81258081	0.00634656			10	0.549103	0.577429983	0.013032725		
11	0.558827	0.577567327	0.01302937			11	0.380923	0.400573957	0.016595369		
12	0.440522	0.455294955	0.015675752			12	0.290152	0.305120286	0.01766119		
13	0.530644	0.548439207	0.013723401			13	0.403797	0.424627975	0.016214777		
14	0.781346	0.807548527	0.006506322			14	0.65633	0.690188581	0.010041951		
15	0.944063	0.97572226	0.000861735			15	0.879028	0.924375068	0.0026478		
16	0.975702	1.008422278	-0.000301426			16	0.942273	0.990882734	0.000324871		
17	1.040039	1.074916826	-0.002723919			17	1.01267	1.064911356	-0.00235471		
18	1.038876	1.073714825	-0.002679479			18	1.019987	1.072605824	-0.002638498		

A5 Data Sheets

AoA	Case 1			Case 2			Case 3			Case 4		
	Axial (N)	Normal (N)	Pitch M(Nm)	Axial (N)	Normal (N)	Pitch M(Nm)	Axial (N)	Normal (N)	Pitch M(Nm)	Axial (N)	Normal (N)	Pitch M(Nm)
-4	0.17415	0.42675	-0.0096975	0.30385	0.3442	-0.0262105	1.0327	4.72005	0.064734	0.9956	3.47775	0.017133
-2	0.21355	0.9194	0.010989	0.29175	0.7998	-0.0009965	1.0132	5.74075	0.0958795	1.09845	4.29285	0.0378885
0	0.113	1.58285	0.038965	0.2324	1.25165	0.0247935	0.7622	6.47145	0.1222245	1.00935	4.77065	0.05768
2	0.19685	2.15215	0.061971	0.2471	1.54485	0.037945	0.74575	6.975	0.1441425	0.95215	5.61225	0.087393
4	0.11115	2.88725	0.089887	0.22035	2.2712	0.0638085	0.66475	7.55235	0.166484	0.847	6.20535	0.1141545
6	0.04095	3.4499	0.1121425	0.10715	2.9553	0.090857	0.45665	8.19355	0.1894135	0.7624	7.2843	0.1540875
8	-0.0613	4.05685	0.137331	-0.0425	4.03965	0.132572	0.34215	8.35475	0.1995605	0.6119	8.07945	0.187982
10	-0.18015	4.4267	0.1527335	-0.2597	4.86995	0.1661435	0.66605	7.62705	0.143461	0.36605	8.78745	0.2185815
12	-0.25075	4.57235	0.1565705	-0.4345	5.6384	0.1975025	0.77275	7.6827	0.1415805	0.02715	9.743	0.25646
14	0.07635	4.0747	0.119983	-0.45245	6.44015	0.229558	1.17075	7.3162	0.1056335	-0.2543	11.118	0.300937
16	0.12705	4.2459	0.1179305	-0.74635	7.00885	0.2538895	1.31235	7.6591	0.111298	-0.57375	11.4047	0.320489
18	0.04645	4.39065	0.1234185	-1.49525	9.17285	0.338112	1.5226	7.949	0.1162595	-0.9455	12.1409	0.3504265
20	0.33445	4.4907	0.1158805	-1.49845	8.8465	0.3272325	1.57035	8.28785	0.121134	-1.1562	12.5071	0.36922

AoA	Case 1			Case 2			Case 3			Case 4		
	Lift (N)	Drag (N)	Pref(Nm)	Lift (N)	Drag (N)	Pref(Nm)	Lift (N)	Drag (N)	Pref(Nm)	Lift (N)	Drag (N)	Pref(Nm)
-4	0.437858548	0.143957204	-0.027180893	0.364557051	0.279099658	-0.040311927	4.780589706	0.700930351	-0.128640312	3.538727921	0.750579192	-0.125345896
-2	0.926292714	0.181333314	-0.026677623	0.809494712	0.263659656	-0.033763266	5.77261306	0.8122335	-0.139311565	4.328570264	0.94796255	-0.137973984
0	1.58285	0.113	-0.025882307	1.25165	0.2324	-0.026484973	6.47145	0.7622	-0.142902394	4.77065	1.00935	-0.137767329
2	2.143969002	0.271839036	-0.026199788	1.535285253	0.300863961	-0.025345496	6.944724719	0.988719699	-0.141614183	5.575601613	1.147434676	-0.142533587
4	2.872463372	0.312283623	-0.028399879	2.250296632	0.378244142	-0.029239611	7.487582239	1.189956007	-0.142925961	6.131150346	1.277800085	-0.140070623
6	3.426720646	0.401338417	-0.029195418	2.927910333	0.415475989	-0.030217799	8.100931953	1.310607614	-0.146265592	7.164703342	1.519640178	-0.144340801
8	4.025900326	0.503900962	-0.028872871	4.006251261	0.520124224	-0.032927209	8.225824071	1.501576685	-0.142722746	7.915661328	1.730387142	-0.143022563
10	4.390731199	0.591275271	-0.028622644	4.841060949	0.589903369	-0.033372021	7.395519604	1.980354537	-0.169009323	8.590384974	1.886413557	-0.141428903
12	4.524567039	0.705374509	-0.030752735	5.605525062	0.747284145	-0.033495418	7.354150813	2.353186706	-0.173169731	9.524447272	2.052240311	-0.142698044
14	3.935193259	1.059841227	-0.046952162	6.358307583	1.119002995	-0.034286573	6.815647533	2.905922694	-0.194101703	10.84926862	2.442941432	-0.154553007
16	4.046401309	1.292456948	-0.056018503	6.943060978	1.214463215	-0.033253973	7.000666771	3.372645859	-0.20248537	11.1210482	2.592037454	-0.146746733
18	4.161402454	1.400962042	-0.056460723	9.185956426	1.412499281	-0.03768774	7.089438972	3.90445474	-0.209400696	11.83885763	2.852520491	-0.14697039
20	4.105489015	1.850190055	-0.068097641	8.825490854	1.61759879	-0.035197105	7.250940155	4.310257952	-0.21840844	12.14827327	3.191207526	-0.143179628

AoA	Case 1			Case 2			Case 3			Case 4		
	CL	CD	CM	CL	CD	CM	CL	CD	CM	CL	CD	CM
-4	0.099366202	0.032669182	-0.069385195	0.082731398	0.063337974	-0.102905041	1.084891561	0.159066866	-0.328382636	0.803067466	0.170334013	-0.319972916
-2	0.210209872	0.041151196	-0.068100488	0.183704111	0.059834069	-0.086188149	1.310018132	0.184325643	-0.355623349	0.982311731	0.215127554	-0.352208881
0	0.359206858	0.025643854	-0.06607027	0.284045402	0.052740104	-0.067608708	1.468609926	0.172971202	-0.364789729	1.082635876	0.229058623	-0.351681348
2	0.486545389	0.061690271	-0.066880709	0.348412668	0.068277094	-0.064699943	1.576013359	0.22437685	-0.361501287	1.265308991	0.260395113	-0.363848268
4	0.651867544	0.070868635	-0.072496925	0.510675037	0.085837502	-0.074640527	1.699207689	0.270044766	-0.364849891	1.391383423	0.289979817	-0.357561011
6	0.777648897	0.091078442	-0.074527714	0.664450498	0.094286777	-0.077137565	1.838399288	0.297425052	-0.37337503	1.625934596	0.344862225	-0.36846158
8	0.913624795	0.114353654	-0.07370434	0.9091657	0.118035309	-0.084053929	1.866741902	0.340762955	-0.364331139	1.796354572	0.39268846	-0.365096488
10	0.996418333	0.134182097	-0.073065583	1.098614709	0.133870762	-0.085189408	1.678315292	0.449415252	-0.431433398	1.949474173	0.428096589	-0.36102832
12	1.026790605	0.160075409	-0.078503108	1.272099722	0.169586246	-0.085504407	1.668927193	0.534024578	-0.442053753	2.161447249	0.465728777	-0.364268082
14	0.893040027	0.240516939	-0.11198557	1.442933752	0.253942919	-0.087524005	1.546721	0.659460695	-0.495487205	2.462097921	0.554393225	-0.394530476
16	0.918277222	0.293305998	-0.142999527	1.575635795	0.275606353	-0.084888066	1.588708668	0.76537734	-0.516888355	2.523774698	0.588228594	-0.374603248
18	0.944375209	0.317929793	-0.144128388	2.084631232	0.320548017	-0.096206229	1.608854344	0.886064327	-0.534541243	2.686672047	0.647341771	-0.375174182
20	0.931686395	0.419876145	-0.173834177	2.002828341	0.367092636	-0.089848336	1.6455049	0.978155995	-0.557535487	2.756889832	0.724202312	-0.36549743

	dist	1.75cm					
Re	Density (kg/m^3)	Chord (m)	Dynamic V	Velocity (m/s)	D Press (mbar)	Corrected Q (mbar)	
100000		1.085	0.0889	1.81E-05	1.876494E+01	1.91E+00	1.98E+00
Q (pa)	S (m^2)	C (m)	A (m)				
197.6015	0.0223	0.012	0.028969				